LAWRENCE
LIVERMORE
NATIONAL
LABORATORY

LLNL-JRNL-823824

The Influence of LiH and TiH2 on Hydrogen Storage in MgB2 I: Promotion of Bulk Hydrogenation at Reduced Temperature

J. L. Snider, Y. S. Liu, A. M. Sawvel, L. Wan, V. Stavila, T. M. Mattox, P. Wijeratne, M. D. Allendorf, B. C. Wood, L. E. Klebanoff

June 24, 2021

International Journal of Hydrogen Energy

Disclaimer

The Influence of LiH and TiH_2 on Hydrogen Storage in MgB_2

I: Promotion of Bulk Hydrogenation at Reduced Temperature

J.L. Snider[1], Y.-S. Liu[2], A.M. Sawvel[3], L.F. Wan[3], V. Stavila[1], T.M. Mattox[4], P. Wijeratne[1], M.D. Allendorf[1], B.C. Wood[3] and L.E. Klebanoff[1]*

[1]*Sandia National Laboratories, Livermore, CA 94551-0969, USA*
[2]*Advanced Light Source, Lawrence Berkeley National Laboratory, Berkeley, CA 94720 USA*
[3]*Lawrence Livermore National Laboratory, Livermore, CA 94551, USA*
[4]*Molecular Foundry, Lawrence Berkeley National Laboratory, Berkeley, CA 94720 USA*

**Corresponding Author: L.E. Klebanoff, Tel: 925-294-3471; email: lekleba@sandia.gov*

Abstract

$Mg(BH_4)_2$ is an attractive hydrogen storage material, owing to its high gravimetric capacity of 14.9 wt. %. However, the dehydrogenated material MgB_2 is very difficult to rehydrogenate, requiring excessive pressures and temperatures. Here we report the influence of LiH and TiH_2 on hydrogen storage reactions involving Bulk MgB_2 using XRD, XAS, FTIR and NMR. In ball-milled mixtures of LiH/MgB_2, the LiH loses crystallinity but remains undissociated, forming a weakly bound complex with MgB_2. The weak interactions produce minor variations in the local electronic structure at B and Mg, but do not markedly affect the underlying MgB_2 hexagonal crystal structure. No evidence is found for a mixed-metal boride $Mg_{1-x}Li_xB_2$ in the as-prepared LiH/MgB_2 materials. The presence of LiH dramatically improves the hydrogenation of MgB_2 at 700 bar, forming borohydride 100 ºC below the minimum hydrogenation temperature of pure MgB_2 and without the formation of undesirable intermediates such as $[B_3H_8]^-$, $[B_{10}H_{10}]^{2-}$ or $[B_{12}H_{12}]^{2-}$. Evidence is reported for a mixed-metal borohydride of the type $Mg_{(3-x)/2}Li_x(BH_4)_3$ produced by the hydrogenation. Subsequent desorption is also improved compared to pure $Mg(BH_4)_2$ and $LiBH_4$, showing single-step hydrogen release up to ~8 wt.% by 380 ºC, whereas $Mg(BH_4)_2$ and $LiBH_4$ still retain significant amounts of hydrogen at this temperature. The material produced by desorption contains both MgB_2 and Mg metal, revealing the original LiH/MgB_2 system is not fully reversible. In contrast to LiH, TiH_2 is essentially inert when ball-milled with MgB_2, and high-pressure hydrogenation leaves only unreacted TiH_2 and MgB_2. Thus, added TiH_2 provides no benefit to MgB_2 hydrogenation.

Keywords: Hydrogen Storage, Magnesium Diboride, Additive, Lithium Hydride

Introduction

The properties of complex metal hydrides and their dehydrogenated boride counterparts continues to be of high interest for both energy and hydrogen storage technologies [1 – 2]. Among these is magnesium diboride (MgB_2), is a fascinating material, not only for its superconducting properties [3], but also for its ability to store hydrogen in the form of magnesium borohydride $Mg(BH_4)_2$ [4 - 14]. While $Mg(BH_4)_2$ has a high hydrogen gravimetric capacity of 14.9%, once it releases hydrogen to form MgB_2, it is difficult to re-hydrogenate MgB_2 back to $Mg(BH_4)_2$. As first observed by Severa et al. [12] and reviewed by Ray and co-workers [7], the complete conversion of MgB_2 to $Mg(BH_4)_2$ requires excessively high pressures (> 700 bar) and temperatures (~ 400 °C). Although the hydrogenation of MgB_2 to $Mg(BH_4)_2$ is somewhat favorable thermodynamically, it proceeds at a very slow rate, with typical reaction times of 24 hours or longer [5]. For "light-duty" or "heavy-duty" vehicular use of a practical hydrogen storage material, rehydrogenation needs to occur in ~ 5 minutes. However, stationary uses of a hydrogen storage material could have more relaxed kinetic requirements.

This study reports the latest in a series of recent investigations of the hydrogenation of MgB_2, building off our first effort in 2010 [13]. Previously, a combined theory and experimental study [7] revealed that the initial hydrogenation of MgB_2 at ~ 120 bar proceeds via a multi-step process: molecular H_2 dissociation (likely at Mg-terminated MgB_2 sites) followed by migration of atomic hydrogen to defective boron sites, where the formation of stable B-H bonds ultimately leads to the creation of $Mg(BH_4)_2$ complexes. A subsequent study [9] examined the extent to which these steps might be rate-limiting. It was found that H-H bond dissociation does not limit the rate of hydrogenation of MgB_2 because H-H bond cleavage occurs rapidly compared to the initial MgB_2 hydrogenation. This finding argues against trying to improve MgB_2 rehydrogenation kinetics by introducing additives that promote H-H bond breaking. The results also showed that surface diffusion of hydrogen atoms is not a limiting factor for MgB_2 hydrogenation [9]. Instead, it was speculated that it is the intrinsic stability of the extended B-B hexagonal ring structure in MgB_2 that hinders the hydrogenation of this material. The present study is motivated by the possibility of disrupting the B-B hexagonal lattice of MgB_2 using the additives LiH and TiH_2.

Anticipating that a significant amount of additive might be needed to disrupt the B-B ring, beyond the 1 – 5 mole percent typical of "catalytic additives," low-mass additives were chosen so as not to severely degrade the gravimetric performance of the $MgB_2/Mg(BH_4)_2$ hydrogen storage system. LiH has displayed interesting chemical effects in the hydrogen storage properties of $LiBH_4$. These prior studies were motivated by the discovery by Vajo et al. [15] that mechanically milled mixtures of LiH + ½MgB_2 (with 2 - 3 mole percent $TiCl_3$) reversibly stored ~ 9 weight percent hydrogen via the reaction: $LiH + ½MgB_2 + 2H_2 \rightarrow LiBH_4 + ½MgH_2$. Although these systems are "Li-rich" for our present purposes and target an improvement in the

hydrogen storage chemistry of $LiBH_4$, they are relevant to our MgB_2 investigation because of the simultaneous presence of LiH and MgB_2 in the dehydrogenated state of "destabilized" $LiBH_4$.

In studies targeting a better understanding of destabilized $LiBH_4$, 2:1 mixtures of LiH:MgB_2 have been examined [14 – 19]. In investigations of MgB_2 superconductivity, lithium metal combined with MgB_2 has also been studied [20 – 22], where the importance of the ternary boride $Mg_{1-x}Li_xB_2$ was emphasized. This ternary boride has also been proposed for 2:1 LiH/MgB_2 materials subjected to prolonged (24 – 120 hours) ball milling [18, 19]. Such a mixed-metal boride, if present, would be important for understanding the chemistry of LiH/MgB_2 mixtures, not only for destabilized $LiBH_4$ but also for the use of LiH to promote the hydrogenation of MgB_2 to $Mg(BH_4)_2$. Dual-cation species in the hydrogenated state, for example mixed-metal borohydrides such as $Mg_{(3-x)/2}Li_x(BH_4)_3$, have been proposed [23] as an alternative to a physical mixture of the individual borohydrides $LiBH_4$ and $Mg(BH_4)_2$ which could be produced by hydrogenation, or intentionally prepared to make a eutectic mixture [24 - 26]. Dual-cation species may be present in the hydrogenation of LiH/MgB_2 to form $Mg(BH_4)_2$.

There have been prior investigations [27, 28] of the combination of LiH and $Mg(BH_4)_2$ showing a reduced hydrogen desorption temperature. We focus here on the influence of LiH on the rehydrogenation of MgB_2 although we examine as well the desorption from the hydrogenated products that are observed.

To our knowledge there have been no prior studies involving the combination of TiH_2 and MgB_2 alone, although Ti-based additives (including TiH_2) have been investigated for their influence on the 2:1 $LiHB_4$:MgH_2 system [29, 30]. TiH_2 is predicted to produce strong destabilization (i.e., a strong tendency to form TiB_2) when combined with $LiBH_4$ [29, 31], suggesting TiH_2 could be a source of potent B-B ring disruption in MgB_2. In experiments involving $LiBH_4$ and TiH_2 alone, TiH_2 shows no reactivity, with either $LiBH_4$ or the dehydrogenated product B at temperatures up to 500 °C [32]. Similar results are found for the combination of $NaBH_4$ and TiH_2 [33]. Nonetheless, we explore here the influence of TiH_2 on the hydrogenation of MgB_2.

This first study (I) examines the influence of LiH and TiH_2 additives on the hydrogen storage properties of Bulk MgB_2. For this investigation of bulk phenomena, x-ray absorption spectroscopy (XAS), nuclear magnetic resonance (NMR, ^{11}B, ^{1}H, ^{7}Li), X-ray Diffraction (XRD) and Fourier Transform Infrared (FTIR) spectroscopy are used to probe the composition of the "as prepared" materials, the products produced by high pressure (700 bar) hydrogenation and subsequent desorption. We assess the presence of mixed metal borides (i.e., $Mg_{1-x}Li_xB_2$) possibly created upon sample synthesis and mixed metal borohydrides (i.e., $Mg_{(3-x)/2}Li_x(BH_4)_3$) that could be created by hydrogenation. If detected, these species would require modification of the current view of the kinetics and thermodynamics of not only the LiH/MgB_2 system, but in other systems where these species appear, for example $LiBH_4$ destabilized with MgH_2. We also

observed some very interesting phenomena occurring near the surfaces of these materials. These surface phenomena, examined with X-ray Photoelectron Spectroscopy (XPS), are the subject of the second companion study (II) [34].

Experimental Methods

Sample preparation and handling were conducted in an Ar-filled glove-box equipped with a recirculation system that keeps H_2O and O_2 concentrations below 0.1 ppm. Commercial grade MgB_2, LiH and TiH_2 powders were used without further purification. The ball-milled materials were produced by loading tungsten carbide (WC) mill pots with the commercial chemicals and milling with WC balls under argon. More details are provided in the Supporting Information (SI).

Five substances used in the study were:

1. Bulk MgB_2: MgB_2 ball-milled for 2 hours.
2. [Low LiH/MgB_2]: LiH added to MgB_2 and ball-milled for one hour. The mole fraction of LiH to MgB_2 was 0.22.
3. [High LiH/MgB_2]: LiH added to MgB_2 and ball-milled for one hour. The mole fraction of LiH to MgB_2 was 0.43.
4. [Low TiH_2/MgB_2]: TiH_2 added to MgB_2 and ball-milled for one hour. The mole fraction of TiH_2 to MgB_2 was 0.24.
5. [High TiH_2/MgB_2]: TiH_2 added to MgB_2 and ball-milled for one hour. The mole fraction of TiH_2 to MgB_2 was 0.44.

Several other commercial chemicals were used as spectroscopic standards, including B_2O_3, MgO, Mg metal, LiB_2, LiOH and $LiBH_4$ with details given in the SI.

FTIR measurements were made under argon at Sandia National Laboratories (SNL) using an Agilent Technologies Cary 630 instrument housed within the argon glovebox. The wavenumber range of the instrument is 400 – 4000 cm^{-1}. All spectra are reported in absorbance mode using a diamond attenuated total reflectance (ATR) crystal. The spectra of some of the weakly IR absorbing materials show unavoidable sharp artifacts from 1900 to 2200 cm^{-1} due to incomplete background subtraction of the diamond ATR crystal absorption. XRD patterns were collected with an Oxford (currently Rigaku) SuperNova Diffractometer using samples loaded in glass capillaries (Charles Supper, Inc.) and sealed under argon with vacuum grease. XAS measurements at the B and Mg K edges were performed without exposing the samples to air at beamlines (BLs) 6.3.1.2, 7.3.1 and 8.0.1.1 of the Advanced Light Source (ALS), Lawrence Berkeley National Laboratory (LBNL). XAS spectra were collected using total fluorescence yield (TFY) mode, as described previously [35].

Solid-state NMR experiments (^{11}B, ^{7}Li, ^{1}H) were conducted at Lawrence Livermore National Laboratory (LLNL). Experiments were carried out on a Bruker Avance III spectrometer using a

Bruker triple-resonance HXY MAS probe at operating frequencies of 600.09 MHz for ^{1}H NMR, 233.22 MHz for ^{7}Li NMR, and 192.54 MHz for ^{11}B NMR. Solid samples were packed inside the argon glove box in 2.5 mm zirconia rotors with tight-fitting vespel top and bottom caps. The chemical shift scale was referenced externally to TMS at 0.0 ppm for ^{1}H NMR, to 0.1M LiCl at 0.0 ppm for ^{7}Li NMR, and to 0.1M H_3BO_3 at 19.6 ppm for ^{11}B NMR. All analyses were completed within 24 hours of removing the sample from the inert environment to ensure the sample integrity. A 90° pulse length of 3.25 μs was used for the ^{1}H NMR experiments while π/8 tip angles of 1.35 μs and 0.92 μs were used for ^{7}Li and ^{11}B experiments, respectively. A prominent probe background signal was observed in the chemical shift region from 90 to -30 ppm in the ^{11}B NMR experiments. An ^{11}B NMR experiment was performed on a rotor filled with sodium chloride to determine the magnitude of this background signal and to subtract it from the other ^{11}B NMR spectra. ^{1}H and ^{7}Li experiments were carried out at a sample spinning speed of 30 kHz and ^{11}B NMR experiments were carried out at a sample spinning speed of 33 kHz to prevent any overlap of spinning sidebands with the spectral regions of interest.

High-pressure (HP) hydrogenation experiments at SNL were performed at 700 bar H_2 and 280 °C in a HP reactor with a Newport Scientific compressor and a vessel made from 316L stainless steel. Samples were loaded inside the argon glovebox. Hydrogen desorption from hydrogenated samples was studied using the PCTPro 2000 (Setaram, Inc.) at SNL. Hydrogen capacity data are presented as weight percent of H desorbed with respect to the total sample weight: wt.% desorbed = [mass H desorbed]/[(mass H desorbed + mass MgB_2 original sample)] x 100. Desorption measurements into static vacuum were conducted using a temperature ramp of 3 °C/min.

The theoretical calculations performed in the work is based on density functional theory (DFT) [36] as implemented in the Vienna Ab initio Simulation Package (VASP) [37, 38]. Projector-augmented-wave pseudopotentials are used to replace the all-electron ion potentials [39, 40], with a kinetic energy cutoff of 600 eV to truncate the planewave basis set. The LiH/MgB_2 interfacial structure is modeled using a ~ 15.49×10.86×21.52 Å^3 simulation cell, where a k-point sampling of 3×4×1 is used to sample the first Brillouin zone. Based on the generalized gradient approximation of the exchange-correlation functional in DFT [41], the initial LiH/MgB_2 interfacial structure was firstly fully optimized at 0 K, followed by ab initio molecular dynamics (AIMD) sampling at finite temperatures (300 K, 700 K and 1000 K) under NVT ensemble using the Nose-Hoover thermostat [42, 43] and a timestep of 0.25 fs. The AIMD simulations performed at elevated temperatures were meant to enhance the structure sampling of the LiH/MgB_2 interface. Limited theoretical results are presented here, with a comprehensive account to be published separately.

Results and Discussion

Materials Characterization

TiH_2/MgB_2:

The XRD, FTIR and XAS data all show no reaction takes place between TiH_2 and MgB_2 upon ball milling, even though TiB_2 formation via the potential reaction: $TiH_2 + MgB_2 \rightarrow TiB_2 + MgH_2$ has a favorable ΔH_{rxn} of -118.38 kJ/mole [44]. Furthermore, high pressure hydrogenation of [Low TiH_2/MgB_2] and [High TiH_2/MgB_2] for 24 hours at 700 bar and 280 °C, a temperature about 100 °C below the threshold for hydrogenation of Bulk MgB_2, yielded only unreacted TiH_2 and MgB_2. Thus, despite the thermodynamic potential for TiH_2 to disrupt the B-B ring of MgB_2 and the elevated temperature, no reaction was observed. The lack of reaction upon ball-milling is presumably due to a high activation energy for this reaction, which likely involves a high barrier for TiH_2 dissociation. Thus TiH_2 is not a useful way of introducing Ti species, which prior studies [15, 29, 30] have been shown to be an active additive for hydrogen storage.

Characterization results for the [Low TiH_2/MgB_2] and [High TiH_2/MgB_2] samples are given in the SI (Figs. S1-S7). The [Low TiH_2/MgB_2] and [High TiH_2/MgB_2] samples served as useful control samples, as these materials were processed identically to the LiH/MgB_2 samples with respect to synthesis, handling, characterization, hydrogenation and material storage. Selected results for these control samples are presented as needed.

LiH/MgB_2: The "As-prepared" Materials

XRD data for the "as prepared" [Low LiH/MgB_2] and [High LiH/MgB_2] samples are shown in Fig. 1, indicating a loss of LiH crystallinity, but no other crystallographic changes. The prominent LiH (200) peak at 44.4 degrees is barely detected, indicating almost complete elimination of crystalline LiH. Comparison of the MgB_2 (101) peak at 42.5 degrees in Fig. 1(b) shows no significant variation in peak position with addition of Li, indicating that a mixed metal boride of the type $Mg_{1-x}Li_xB_2$ has not formed in the "as prepared" samples and that the underlying MgB_2 hexagonal lattice is maintained. Zhao et al. reported [22] XRD measurements of Li-Mg boride synthesized by melting Li metal, B and Mg metal together at 950 °C and found that the "a axis" (within the B-B plane) decreases with the introduction of Li as evidenced by a shift of the (101) and (100) peaks to larger 2θ while the (002) peak remains constant. We find no evidence for this lattice effect in the as-prepared ball-milled LiH/MgB_2 materials. A comparison (not shown) of the XRD for [Low LiH/MgB_2] and [High LiH/MgB_2] with that of standard LiB_2 powder revealed no evidence for the formation of a crystalline LiB_2 phase in the "as-prepared" LiH/MgB_2 samples.

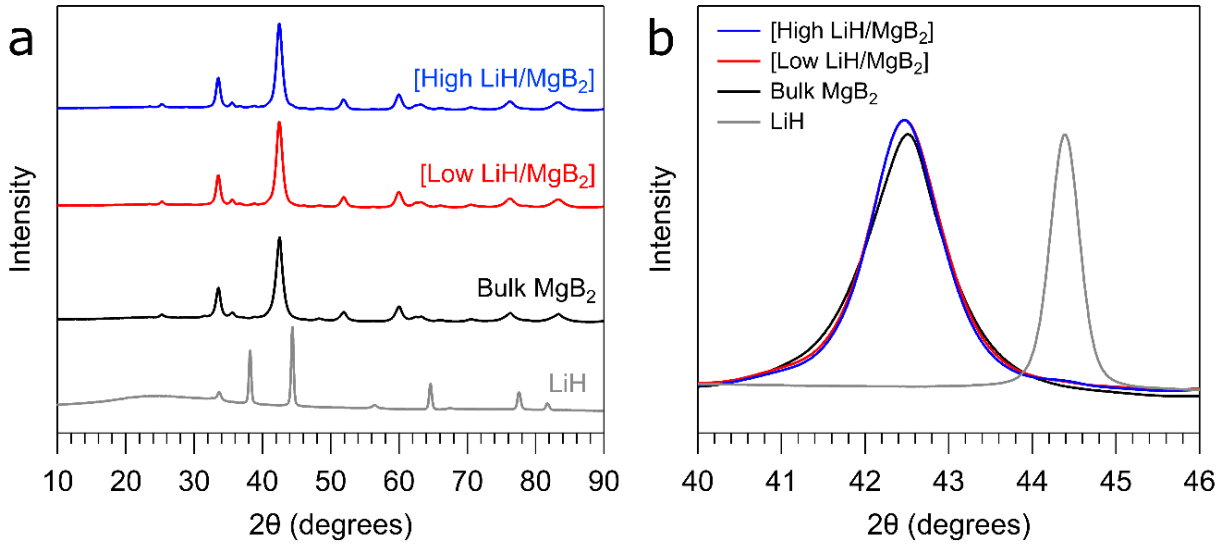

Fig. 1: a) XRD patterns of commercial (bulk) LiH, Bulk MgB_2, [Low LiH/MgB_2] and [High LiH/MgB_2]. The data has been shifted vertically for clarity; (b) XRD data with an expanded abscissa scale near the MgB_2 (101) peak for the various samples.

FTIR data were collected for [Low LiH/MgB_2] and [High LiH/MgB_2] and show no production of amorphous reaction products, but does reveal undissociated LiH. The FTIR spectra in Fig. 2(a) do not show the presence of partially hydrogenated boron species (e.g., $[B_3H_8]^-$, $[B_{10}H_{10}]^{2-}$ or $[B_{12}H_{12}]^{2-}$) which would present absorbance peaks in the 2400 – 2500 cm^{-1} range [7]. Such species could have arisen from the possible reaction of LiH with MgB_2.

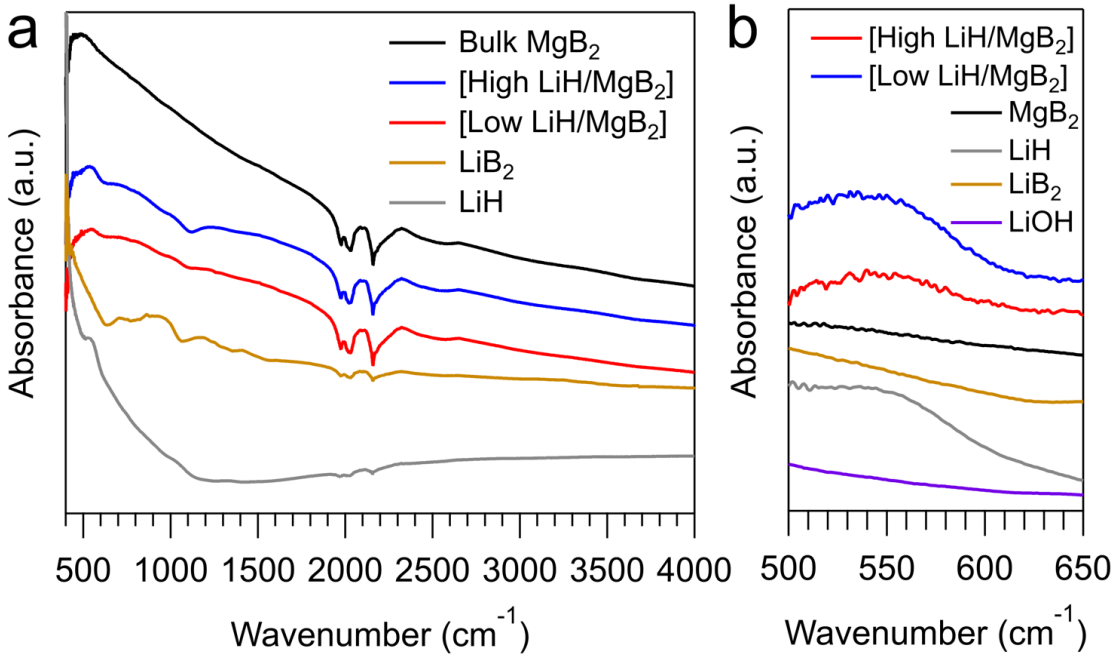

Fig. 2: (a) FTIR spectra for LiH, LiB_2 and Bulk MgB_2 standards, along with [Low LiH/MgB_2] and [High LiH/MgB_2] from 400 – 4000 cm^{-1}; (b) same data plotted with an expanded abscissa from 500 – 650 cm^{-1} with the addition of data from LiOH standard powder. The LiH/MgB_2 data have been scaled by a factor of 8.8 in panel 2(b) to increase the prominence of this feature on the elevated spectral background in order to compare with Bulk LiH.

Fig. 2(b) shows a 550 cm^{-1} feature which grows in prominence as the LiH content of the LiH/MgB_2 samples increase. The feature is not due to LiOH contamination or LiB_2. Rather, it corresponds to LiH [45, 46], indicating that while the crystalline form of LiH was removed by the ball-milling (Fig. 1(b)), LiH remains, either in amorphous form or as particles too small to support the diffraction of x-rays.

NMR was used on selected samples to further clarify chemical species in the "as prepared" LiH/MgB_2 materials. Fig. 3 presents results from ^{7}Li, ^{11}B and ^{1}H NMR for the [Low LiH/MgB_2] and [High LiH/MgB_2] samples, along with comparison to a LiB_2 standard.

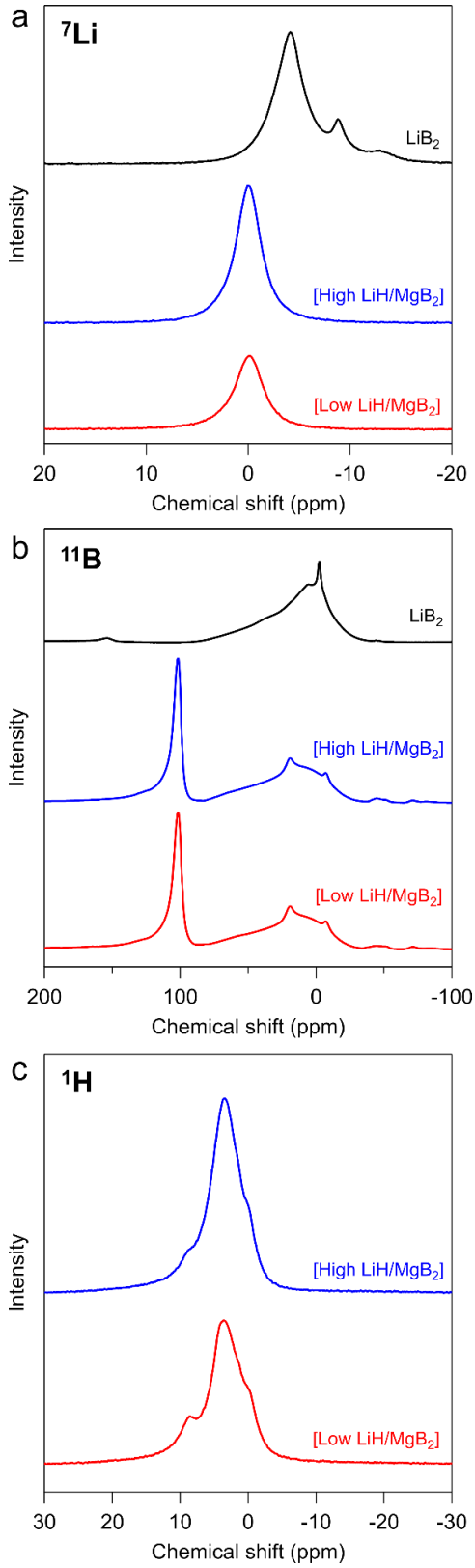

Fig. 3: (a) ^{7}Li, (b) ^{11}B and (c) ^{1}H NMR spectra for [Low LiH/MgB_2] and [High LiH/MgB_2] compared to a standard LiB_2 sample powder.

The ^{7}Li NMR data in Fig. 3(a) reveals a single common Li species for both the [Low LiH/MgB_2] and [High LiH/MgB_2] samples. The peak at -0.05 ppm agrees well with literature reports for LiH [47], thereby confirming the FTIR results indicating the presence of undissociated LiH in the [Low LiH/MgB_2] and [High LiH/MgB_2] samples. The poor correspondence to LiB_2 confirms the LiH did not react with MgB_2 to form LiB_2.

The ^{11}B spectra in Fig. 3(b) for [Low LiH/MgB_2] and [High LiH/MgB_2] show a boride-like feature at 101.5 ppm, but it is shifted to higher ppm than the corresponding peak in Bulk MgB_2 at 98 ppm [35]. This suggests an electronic modification at B in the LiH/MgB_2 samples. In agreement with the FTIR findings (Fig. 2), no evidence is found for previously identified hydrogenated boron species which would be found at -41 ppm ($[BH_4]^-$) [35, 48], -12 to -16 ppm ($[B_{12}H_{12}]^{2-}$) [49, 50], -37 ppm ($[B_4H_{11}]^{3-}$) [51] and -31 ppm ($[B_{10}H_{10}]^{2-}$)[35]. There is a small feature at -8.2 ppm that could not be identified but could be a previously uncharacterized B_xH_y species with low H content. There is also a small peak at 19 ppm which corresponds to boron hydroxide (i.e., boric acid) [52], shifted to higher ppm than the peak position reported for the hard oxide B_2O_3 (14.6 ppm) [53]. Boron hydroxide was found in the B 1s XPS data for [Low LiH/MgB_2] and [High LiH/MgB_2], as will be reported in (II) [34].

The ^{1}H NMR for [Low LiH/MgB_2] and [High LiH/MgB_2] are very similar. The main peak at 3.5 ppm corresponds to LiH, consistent with prior studies [47]. The main peak is accompanied by smaller features at ~ 0.1 ppm and 8.4 ppm which could not be definitively identified. The 8.4 ppm feature is likely hydroxylated B, as was found in the XPS study of (II) [34].

Even though LiH has not reacted with MgB_2, B K-edge XAS was used to assess possible influences on the B-B ring. The results, shown in Fig. 4, indicate only a very small influence on the B-B ring structure.

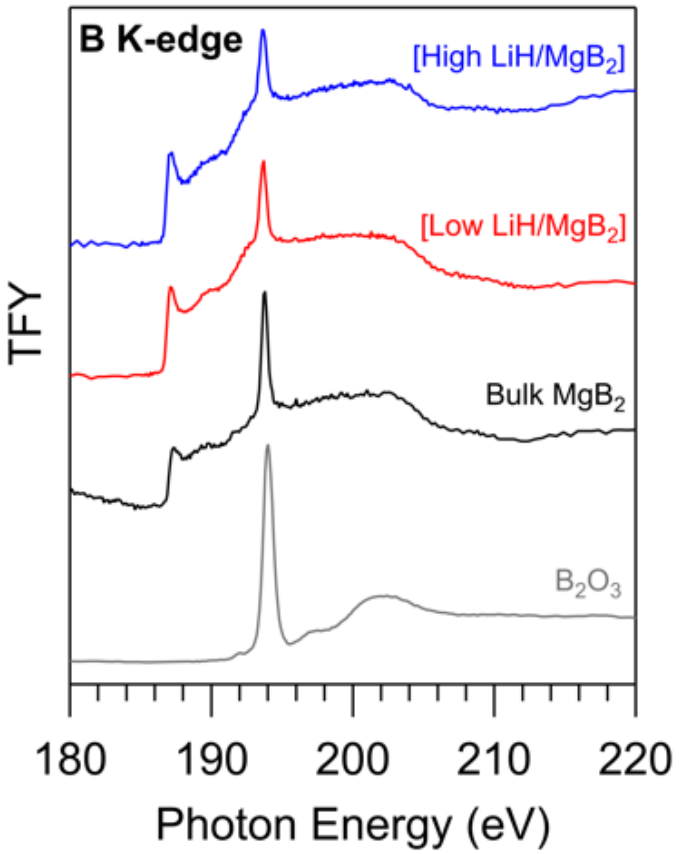

Fig. 4: Boron K-edge TFY XAS data for Bulk MgB_2, [Low LiH/MgB_2] and [High LiH/MgB_2] along with data for B_2O_3 standard powder. The depth sensitivity of the B K-edge TFY measurement is estimated to be 135 nm.

The B $2p_{xy}$ feature at 187.2 eV photon energy is the XAS signature for the B-B network in MgB_2. Significant disruptions of the B-B ring, for example oxidizing boron completely to B_2O_3, eliminates the intensity of the B K-edge $2p_{xy}$ feature, as shown in Fig. 4. An analysis of the intensity of the B $2p_{xy}$ feature (Fig. S8 of the SI) reveals that the addition of LiH causes at most a 10% reduction in the XAS intensity in the B-B ring signature, indicating that although the majority of the B-B network is not significantly disrupted by introducing LiH, a small minority of the B atoms may be affected, as observed in the ab initio molecular dynamics simulations (AIMD) depicted in Fig. 5. Similar phenomena are seen in the Mg K-edge XAS (Fig. S9 of the SI), where added LiH causes a slight modification of the unoccupied electronic structure at the Mg site. These XAS findings are consistent with the XRD data (Fig. 1) that showed retention of the MgB_2 crystallography of [Low LiH/MgB_2] and [High LiH/MgB_2] with no apparent change in the MgB_2 lattice spacings.

The picture emerging from the data on the "as prepared" LiH/MgB_2 is captured in Fig. 5, which is the result of an AIMD calculation for explicit modeling of the LiH-MgB_2 interactions. A

comprehensive account of this theoretical work on LiH-MgB_2 interaction and its impact on the initial hydrogenation of MgB_2 will be given in a future publication.

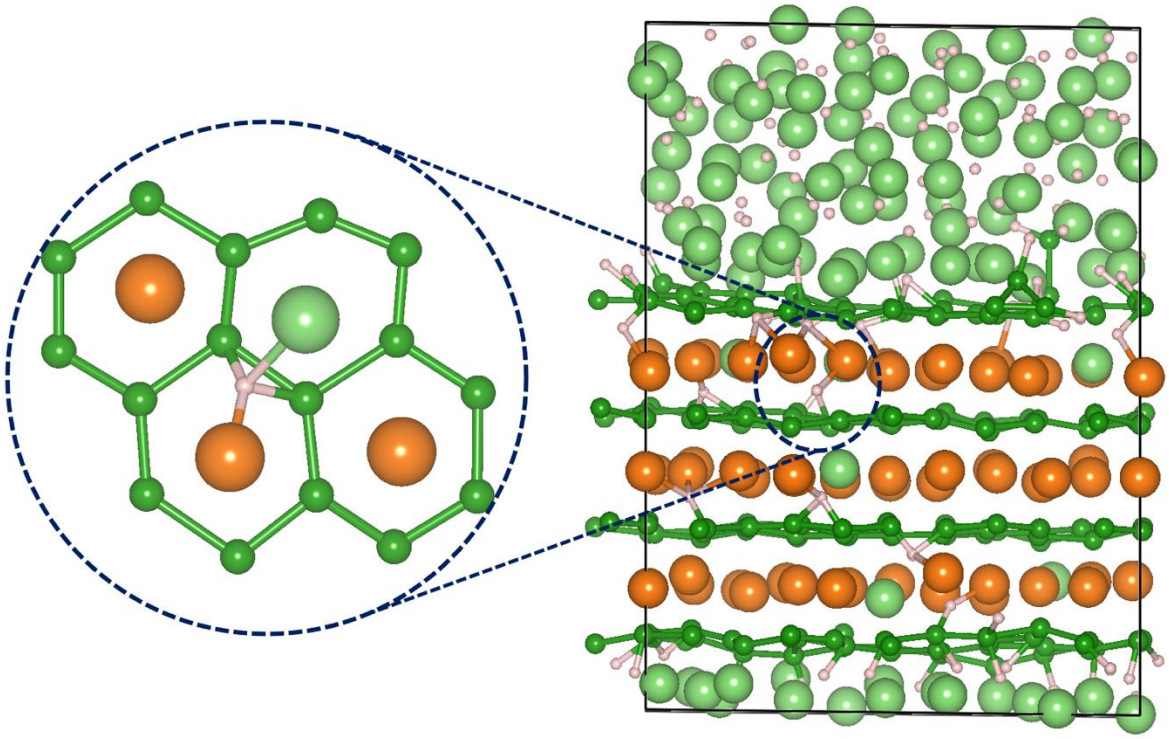

Fig. 5: Schematic diagram of intact LiH molecules interacting with B and Mg atoms in MgB_2 for the as-prepared ball-milled LiH/MgB_2 materials. Legend: Large orange balls = Mg; large light green balls = Li; small dark green balls = B, and small white balls = H.

The LiH/MgB_2 interfacial model, shown in Fig. 5, was initially constructed based on crystalline LiH(111) surface interfacing with the B-terminated MgB_2 basal plane. Partial Li substitution is considered by replacing certain Mg atoms in MgB_2 with Li. The thermodynamics associated with Li substitution will be addressed in the follow-up theory study as well as its potential impact on B-H interactions during initial hydrogenation reactions. In our simulations, we have also considered other interfacial models based on different crystallographic orientations and terminations of LiH and MgB_2. Similar behavior is observed in all models, where LiH quickly losses its crystallinity during AIMD, in agreement with the XRD results discussed in Fig. 1. However, the degree of LiH-MgB_2 interaction varies in the different interfacial models due to variation in the intrinsic reactivity of the different LiH and MgB_2 surfaces. The interfacial model, depicted in Fig. 5, show the strongest interactions between LiH and MgB_2, where a few BH_x bonds are formed right at the LiH/MgB_2 interface and a small fraction of LiH diffuses into the interior of MgB_2. Although the limited interaction between LiH and MgB_2 at the interface is predicted to produce amorphous LiH (as seen in the XRD of Fig. 1(b)), the chemical characteristic of bulk LiH and MgB_2 are mostly preserved, i.e. Li and H remains positively and

negatively charged, respectively and the B-B ring structure is maintained. The MgB_2 structure remains bulk-like where not proximate to LiH. The diffused H in the diffused LiH, as highlighted in the zoom-in plot in Fig. 5, retains its two electrons and predominately resides at the bridging site between two B atoms to form the so called three-center two-electron bond, but with bonding interactions with Mg and Li as well.

Note that Fig. 5 depicts a precursor state for potential lithium substitution of Mg and hydrogenation of B. A system like this could be metastable, mobile and reactive. The companion study (II) [34] will probe the LiH-B and LiH-Mg interactions further with XPS and confirm the metastability, mobility and reactivity of the as prepared LiH/MgB_2 materials at and near their surfaces.

HP Hydrogenation:

Although as-prepared LiH/MgB_2 materials did not have strongly disrupted hexagonal B-B ring networks, we tested if the weak LiH-Mg and LiH-B interactions could lead to an improved MgB_2 hydrogenation. It was decided the most informative test would be to attempt the HP hydrogenation for conditions of temperature and time for which pure MgB_2 does not hydrogenate. In this way, if hydrogenation occurred for the LiH/MgB_2 materials, a significant improvement in hydrogenation would have been shown. Along these lines, we simultaneously exposed Bulk MgB_2, [Low LiH/MgB_2], [High LiH/MgB_2], [Low TiH_2/MgB_2] and [High TiH_2/MgB_2] to 700 bar hydrogen for 24 hours at 280 ºC, 100 ºC below the temperature threshold for Bulk MgB_2 hydrogenation. The experimental arrangement did not allow for the measurement of hydrogen uptake versus time at this high pressure. The materials were examined post-exposure with XRD, FTIR, XAS and NMR.

For the TiH_2/MgB_2 samples, HP hydrogenation yielded only unreacted TiH_2 and MgB_2, with no hydrogenation having taken place (see Figs. S4-S7 of the SI). In contrast, the [Low LiH/MgB_2] did react, turning from a fine black powder into a uniform and hard black mass, difficult to scrape out of the vial. In contrast, the [High LiH/MgB_2] sample converted into a roughly 50-50 (by volume) mixture of an off-white fluffy material on top, and a very hard black mass on the bottom of the vial. We call these two fractions "Top" and "Bottom," respectively. Our labels for the HP hydrogenation materials produced from the original [Low LiH/MgB_2] and [High LiH/MgB_2] samples are: [Low LiH/MgB_2 HP], [High LiH/MgB_2 HP Top] and [High LiH/MgB_2 HP Bottom], respectively.

XRD data of the [Low LiH/MgB_2 HP] material is shown in Fig. 6 (a), which shows evidence of hydrogenation 100 ºC below that of the ball-milled MgB_2. The data indicates that some unconverted MgB_2 remains, along with a primary crystalline phase similar to β-$Mg(BH_4)_2$. However, the borohydride XRD peaks are shifted 0.2° to higher 2θ values than β-$Mg(BH_4)_2$, indicating a decrease in the lattice d-spacing, perhaps due to a partial substitution of Mg with

smaller Li atoms in the $Mg(BH_4)_2$ lattice. Very small XRD peaks observed from 23 - 27° correspond to the presence of *o*-$LiBH_4$ in small amounts. These peaks show a subtle increase in lattice d-spacing, 0.1° shift to lower 2θ values than *o*-$LiBH_4$, which would again be consistent with substitution between Li and Mg atoms.

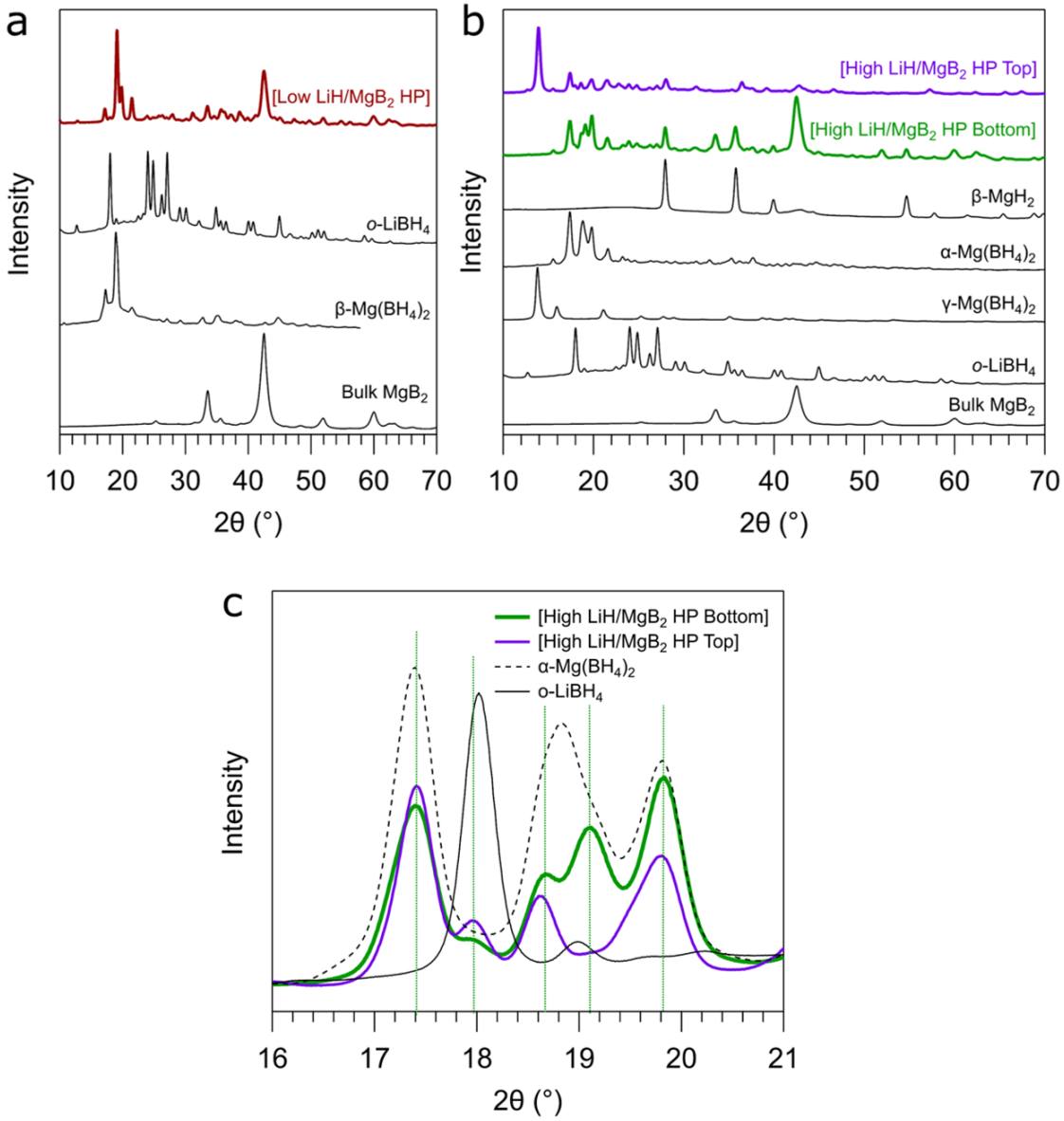

Fig. 6: (a) XRD patterns of [Low LiH/MgB_2 HP] compared to standard powders of Bulk MgB_2, β-$Mg(BH_4)_2$ and o-$LiBH_4$; (b) XRD patterns of [High LiH/MgB_2 HP Top] and [High LiH/MgB_2 HP Bottom] compared to standard powders of Bulk MgB_2, *o*-$LiBH_4$, γ-$Mg(BH_4)_2$, α-$Mg(BH_4)_2$ and β-MgH_2; (c) Comparison of [High LiH/MgB_2 HP Top] and [High LiH/MgB_2 HP Bottom] with standard samples of *o*-$LiBH_4$ and α-$Mg(BH_4)_2$ from 2Θ values 16 – 21 degrees.

The XRD pattern of [High LiH/MgB_2 HP Bottom] shown in Fig. 6 (b) was very similar to that of the [Low LiH/MgB_2 HP] sample, with a significant amount of MgB_2 remaining. Other observed products include β-MgH_2 (peaks at 28° and 35.8°), *o*-$LiBH_4$ (minor peaks from 23-27°), and an apparent α-$Mg(BH_4)_2$ phase (peaks from 17-22°). The low temperature α-phase is not expected to be stable at the hydrogenation conditions [5] and evidence suggests that these peaks are indicative of a mixed metal borohydride phase. The pattern for [High LiH/MgB_2 HP Top] in Fig. 6 (b) was quite different. The off-white material displayed an XRD pattern composed primarily of apparent α- and γ-$Mg(BH_4)_2$ phases with very little unreacted MgB_2 present. Interestingly, both the [High LiH/MgB_2 HP Top] and [High LiH/MgB_2 HP Bottom] samples have peaks similar to those of $Mg(BH_4)_2$ phases that are expected to irreversibly transform to β-$Mg(BH_4)_2$ at the temperature of the hydrogenation.

Fig. 6(c) examines the XRD of [High LiH/MgB_2 HP Top] and [High LiH/MgB_2 HP Bottom] more closely, and provides evidence for a new borohydride phase which may account for these unexpected peaks. Rather than producing a mixture of $Mg(BH_4)_2$ and $LiBH_4$, we see evidence for a mixed metal borohydride, similar to the mixed-metal borohydride reported by Fang et al. [23] when 1:1 mixtures of $LiBH_4$ and $Mg(BH_4)_2$ are ball milled together and heated to 200 °C. These workers found the 5-peak pattern that we observe for [High LiH/MgB_2 HP Bottom]. In comparison, the [High LiH/MgB_2 HP Top] pattern is similarly offset from the $Mg(BH_4)_2$ and $LiBH_4$ standards; however, it lacks the peak at 19.1° which is found in the 5-peak pattern. This suggests that a different mixed-metal phase present in [High LiH/MgB_2 HP Top], which may also include the large peak at 13.9°. The proposed mixed metal borohydride phases are consistent with the observed XRD patterns and the absence of β-$Mg(BH_4)_2$ after heating. Summarizing, these XRD results show that [Low LiH/MgB_2] and [High LiH/MgB_2] materials hydrogenate to form borohydride species 100 ºC below that of the ball-milled MgB_2. Furthermore, there is evidence for a mixed metal borohydride of the type $Mg_{(3-x)/2}Li_x(BH_4)_3$ produced by the hydrogenation.

Fig. 7 displays FTIR data for the HP hydrogenation products, compared to the standard powders α-$Mg(BH_4)_2$ and *o*-$LiBH_4$. The hydrogenated LiH/MgB_2 materials show borohydride stretches in the region 2100 - 2400 cm^{-1} and no evidence for terminal B-H intermediates (B_xH_y) in the range 2400 – 2500 cm^{-1} [7]. A closer inspection of the borohydride region (Fig. S10 of the SI) is inconclusive on the presence of a mixed-metal borohydride. For the [High LiH/MgB_2 HP Top] sample, and to a much lesser extent the [High LiH/MgB_2 HP Bottom] sample, there appear features from 650 – 800 cm^{-1} that correspond to a lithium borate glass [53]. This is a consequence of surface carbonate contamination, and will be discussed fully in the companion study (II) [34]. Fig. 7(b) shows that upon HP hydrogenation, the molecular LiH feature at 550 cm^{-1} disappears, signaling reaction of LiH with MgB_2.

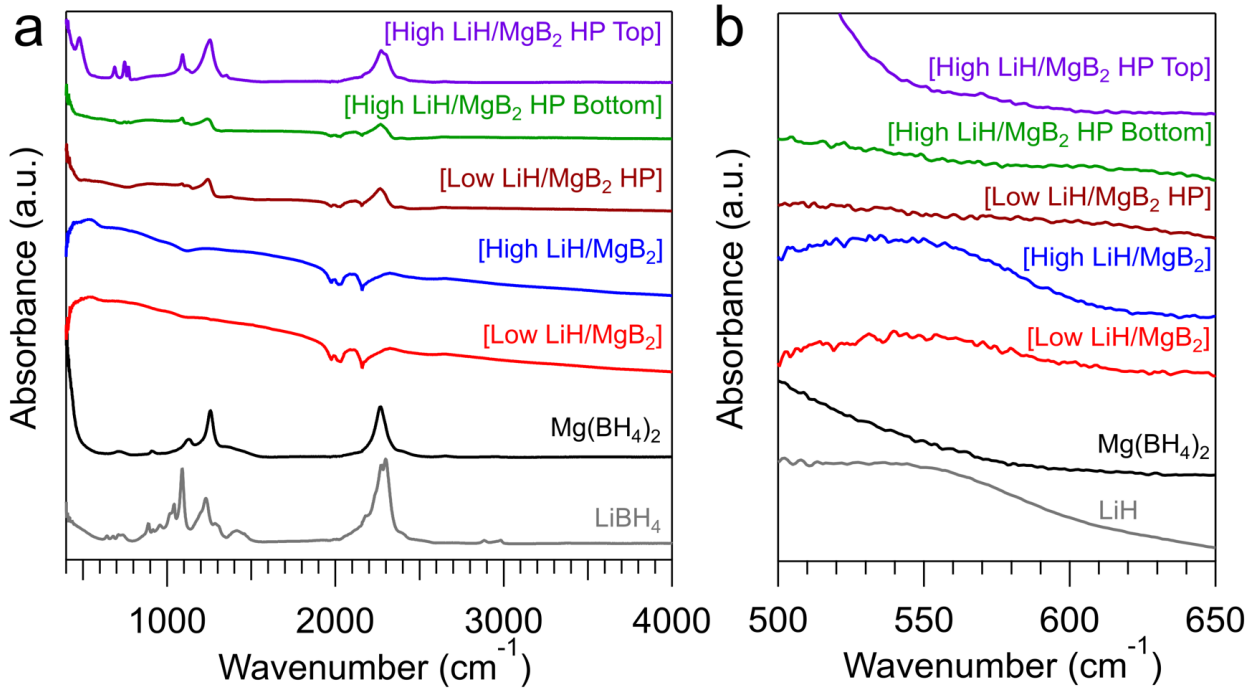

Fig. 7: (a) FTIR data of the original samples [Low LiH/MgB_2] and [High LiH/MgB_2] along with hydrogenated samples [Low LiH/MgB_2 HP], [High LiH/MgB_2 HP Top] and [High LiH/MgB_2 HP Bottom]. Data are also shown for α-$Mg(BH_4)_2$ and *o*-$LiBH_4$ standards, (b) FTIR data from 500 – 650 cm^{-1}, with the spectrum from standard LiH plotted.

NMR was used to further clarify the chemical identity of the hydrogenated sample [High LiH/MgB_2 HP Top], especially the question of the existence of the mixed-metal borohydride $Mg_{(3-x)/2}Li_x(BH_4)_3$, as shown in Fig. 8. The results confirm the presence of a mixture of borohydrides including the presence of mixed metal borohydrides that are consistent with the x-ray diffraction data in Fig. 6(b).

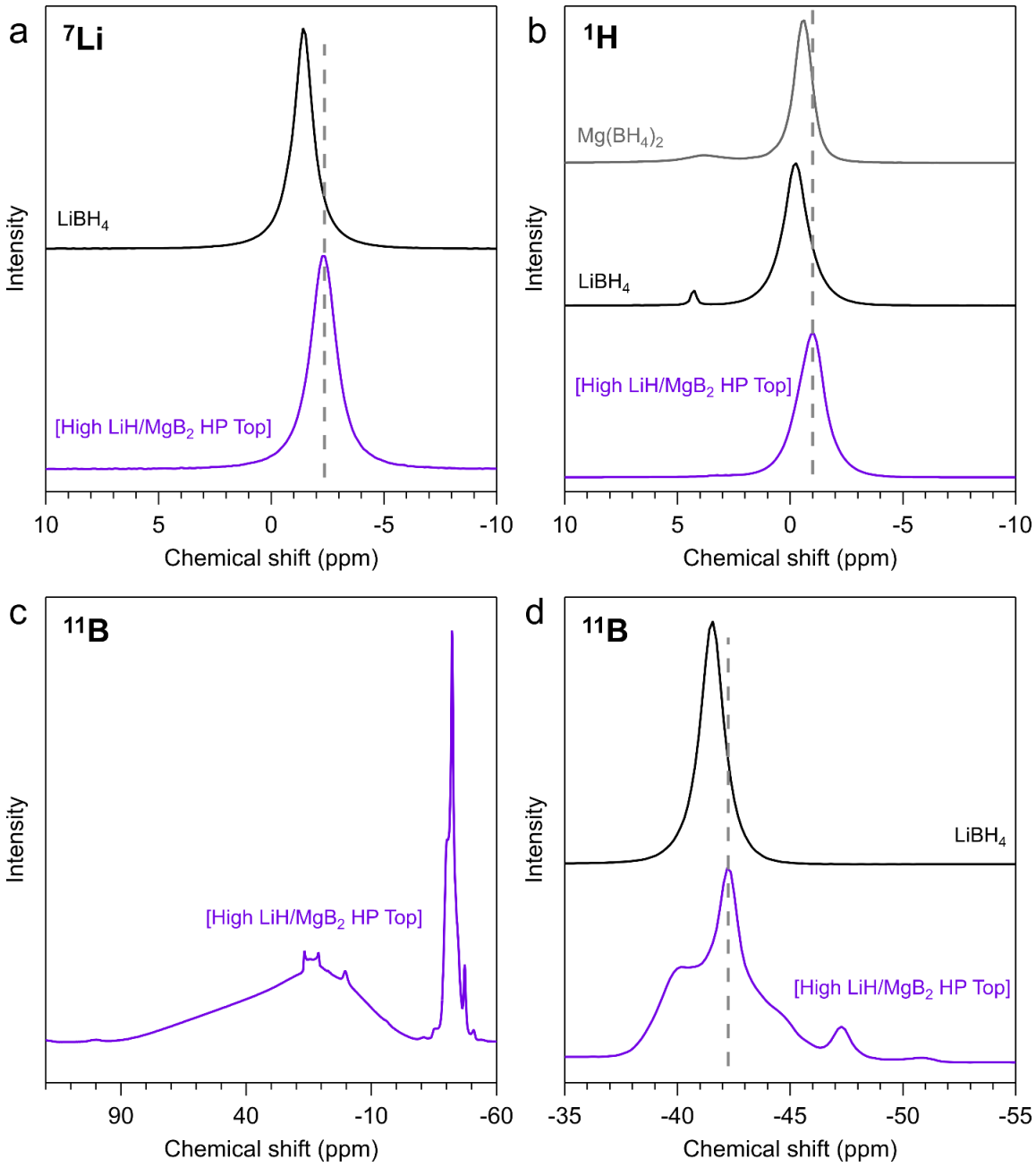

Fig. 8: (a) ^{7}Li, (b) ^{1}H, and (c, d) ^{11}B NMR results for [High LiH/MgB_2 HP Top] compared to standard powders of *o*-$LiBH_4$ and α-$Mg(BH_4)_2$.

The ^{7}Li results (Fig. 8(a)) shows that the original LiH peak at -0.05 ppm (Fig. 3(a)) is no longer present, and instead there appears a single broad peak at -2.4 ppm that is shifted significantly away from the pure o-$LiBH_4$ peak at -1.5 ppm. Given the prior XRD results in Fig. 6 which indicated a mixed metal borohydride, we attribute the ^{7}Li peak at -2.4 ppm to the formation of

$Mg_{(3-x)/2}Li_x(BH_4)_3$. However, the broad nature of this peak does not exclude the possibility that other species (e.g., $LiBH_4$) are also contributing to the peak shape and intensity.

The ^1H results in Fig. 8(b) indicate a wholesale transformation from the original ^1H peak at 3.5 ppm characteristic of LiH (Fig. 3(c)) to a single peak at -1.0 ppm for [High LiH/MgB_2 HP Top]. This peak does not solely correspond to either pure $Mg(BH_4)_2$ (at – 0.6 ppm) or pure $LiBH_4$ (at -0.3 ppm). Again, given the prior XRD results, we attribute the ^1H peak at -1.0 ppm to a mixed-metal borohydride $Mg_{(3-x)/2}Li_x(BH_4)_3$. However, the peak is broad and asymmetric, and we cannot exclude from this NMR data alone possible contributions of $Mg(BH_4)_2$ and $LiBH_4$ to the broad lineshape. There is also no indication of the proton NMR signatures of closo-borates $[B_{10}H_{10}]^{2-}$ or $[B_{12}H_{12}]^{2-}$ which would produce ^1H peaks from ~ 0 – 1 ppm [55].

The differing ^7Li and ^1H chemical shifts observed in Fig. 8 between [High LiH/MgB_2 HP Top] and the pure substances $Mg(BH_4)_2$ and $LiBH_4$ cannot be attributed to a spurious effect assuming the presence of a physical mixture composed of $Mg(BH_4)_2$ and $LiBH_4$. Lee and coworkers [56] have shown that the multi-nuclear NMR peak positions for pure $LiBH_4$ and $Ca(BH_4)_2$ are unchanged when $LiBH_4$ is ball milled together with $Ca(BH_4)_2$. The same is likely true for the combination of $LiBH_4$ and $Mg(BH_4)_2$.

The wide-scan ^{11}B spectrum in Fig. 8(c) shows the presence of borohydride in the - 40 to - 50 ppm range, and no evidence for significant production of previously identified hydrogenated B_xH_y species by the HP hydrogenation, which would manifest at -12 to -16 ppm ($[B_{12}H_{12}]^{2-}$) [49, 50], -37 ppm ($[B_4H_{11}]^{3-}$) [51] and -31 ppm ($[B_{10}H_{10}]^{2-}$)[35]. There is a small feature at 13.6 ppm that indicates a B-O species, not too far from the 14.6 ppm reported [53] for the hard oxide B_2O_3. There is also a small feature at 0.27 ppm that may represent a small amount of a BO_4 species.

A closer look at the ^{11}B borohydride region in Fig. 8(d) compares the data for [High LiH/MgB_2 HP Top] with standard o-$LiBH_4$. Qualitative analysis of the ^{11}B data show four broad peaks for [High LiH/MgB_2 HP Top] centered near -40.2 ppm, -42.2 ppm, -44.6 ppm, and -47.2 ppm. The broad peak centered near -40.2 ppm is consistent with previously reported [28, 48] chemical shift values for $Mg(BH_4)_2$ and confirms the presence of $Mg(BH_4)_2$ in [High LiH/MgB_2 HP Top]. The broad peak centered near -42.2 ppm is shifted by roughly 0.7 ppm from the o-$LiBH_4$ standard (-41.5 ppm). If this were $LiBH_4$, a possible explanation for the shift could be that the $LiBH_4$ in the [High LiH/MgB_2 HP Top] sample is in the proximity of or coordinated to an electronically shielding species, such as that reported by Yan et al. [57] for $LiBH_4$-$Co_{1.34}B$, which produced a $LiBH_4$ peak shifted to -41.9 ppm. Alternatively, Ravnsbaek and coworkers have noted [58] that for mixed-metal M-Zn borohydride phases where M is an alkali metal, the mixed metal borohydrides exhibit ^{11}B NMR shifted to lower (i.e., more negative) ppm than those of the pure alkali metal borohydrides (MBH_4). The assignment of this feature needs follow-on work, but it is likely amorphous since the x-ray diffraction data of [High LiH/MgB_2 HP Top] didn't show any reflections consistent pure $LiBH_4$.

The two peaks in Fig. 8(d) at -44.5 and -47.3 ppm display more distinct chemical shift differences from the $LiBH_4$ standard (-41.5 ppm). We assign these peaks to the presence of mixed metal borohydrides such as $Mg_{(3-x)/2}Li_x(BH_4)_3$. Ravnsbaek et al. report [59] $LiZn_2(BD_4)_5$ shows a ^{11}B NMR peaks at -46 ppm which could be analogous to the ^{11}B feature at -47.3 ppm in Fig. 8(d). While singular, broad peaks are observed for both the ^{7}Li and the ^{1}H NMR data, the ^{11}B NMR data indicates a mixture of borohydrides of varying amounts and types including the presence of mixed metal borohydrides that are consistent with the x-ray diffraction data in Fig. 6(b).

The effect of the HP hydrogenation on the B-B ring of MgB_2 was examined with B K-edge XAS, as shown in Fig. 9. In contrast to the XAS data (Fig. 4) for the as-prepared precursor state of Fig. 5, the HP hydrogen treatment produces dramatic changes in the B unoccupied electronic structure.

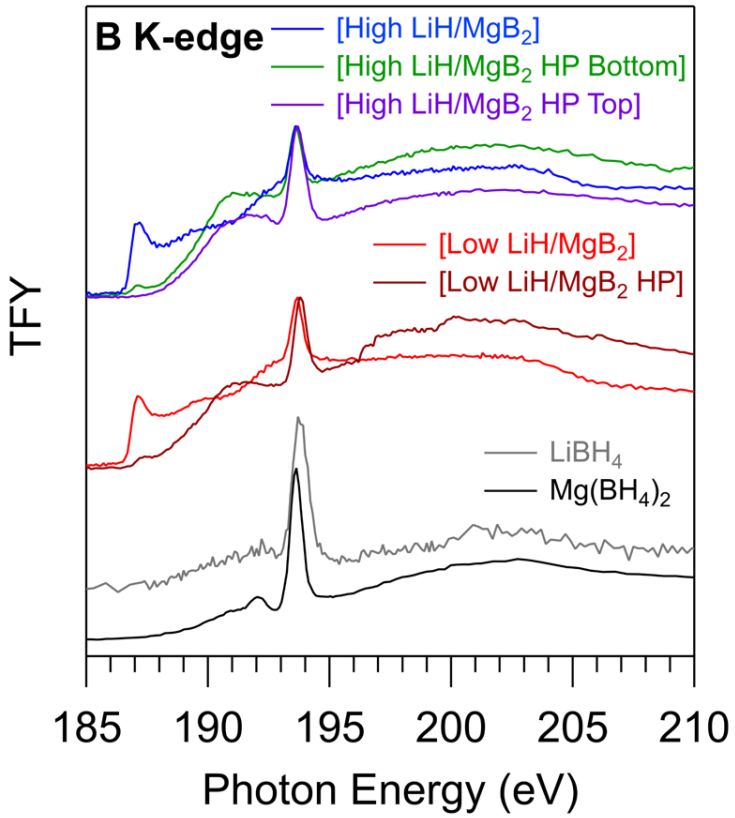

Fig. 9: Boron K-edge TFY XAS data for original [Low LiH/MgB_2] and [High LiH/MgB_2] samples along with data for the HP hydrogenated samples [Low LiH/MgB_2 HP], [High LiH/MgB_2 HP Top] and [High LiH/MgB_2 HP Bottom]. These spectra are compared to those obtained from pure α-$Mg(BH_4)_2$ and *o*-$LiBH_4$.

The B $2p_{xy}$ feature at 187.2 eV photon energy in Fig. 9, signature for the B-B ring in MgB_2, is almost completely removed in the [Low LiH/MgB_2 HP] and [High LiH/MgB_2 HP Bottom] samples and is completely removed in the [High LiH/MgB_2 HP Top] sample. Similar results are seen for Mg K-edge XAS for these samples (Fig. S11 of the SI). In addition, B K-edge TFY intensity for all three hydrogenated LiH/MgB_2 samples starts to grow in at the general position of the $Mg(BH_4)_2$ and $LiBH_4$ but does not reproduce them in detail. For example, the $Mg(BH_4)_2$ peak at 192.2 eV is not seen. Additional B K-edge XAS spectra shown in the SI (Fig. S12) indicate there is no evidence for elemental B, $[B_{12}H_{12}]^{2-}$ or $[B_{10}H_{10}]^{2-}$ which could have been produced as hydrogenation intermediates, consistent with the FTIR and NMR findings.

The production of borohydride by the HP hydrogenation of the LiH/MgB_2 materials introduces the possibility of eutectic formation in the product phase. Bardaji and co-workers [26] found that ball-milled mixtures of $xLiBH_4$ and $(1-x)Mg(BH_4)_2$ form a eutectic for $0.33 < x < 0.66$. The eutectic mixture melts at 180 °C, well below both the melting points of pure $LiBH_4$ and $Mg(BH_4)_2$, and also below the 280 °C temperature of the HP hydrogenation.

Eutectic melting explains the physical characteristics of the Li/MgB_2 HP hydrogenation products. For the [Low LiH/MgB_2] sample, the Li/Mg ratio is 0.22, which corresponds to an x value of 0.18. Even if the entire sample were hydrogenated to the pure substances $LiBH_4$ and $Mg(BH_4)_2$ (as opposed to the mixed-metal borohydride), the relative amounts of Li and Mg are inconsistent with the eutectic composition range, and no melting occurs. This explains why the product [Low LiH/MgB_2 HP] was a single-phase material. However, for the [High LiH/MgB_2] sample, the Li/Mg ratio is 0.43, which corresponds to an x value of 0.30. This value of x is close to the lower end of the eutectic range $0.33 < x < 0.66$. Since two material phases [High LiH/MgB_2 HP Bottom] and [High LiH/MgB_2 HP Top] were produced as a result of the HP hydrogenation of [High LiH/MgB_2], it seems likely that eutectic melting of borohydride product occurred. As $LiBH_4$ and $Mg(BH_4)_2$ were being produced at 280 °C in the HP hydrogenation of [High LiH/MgB_2], the product mixture melted, and floated to the top of the sample, leaving behind an un-melted phase with composition insufficient to support eutectic melting. This would naturally explain the creation of the white-fluffy [High LiH/MgB_2 HP Top] material on top of the hard black [High LiH/MgB_2 HP Bottom] material. It may also be that the initial creation of a eutectic liquid phase, promotes the complete MgB_2 hydrogenation seen for [High LiH/MgB_2 HP Top].

Summarizing the HP hydrogenation results, [Low LiH/MgB_2] and [High LiH/MgB_2] samples hydrogenate to borohydride 100 ºC below that of the Bulk MgB_2. However, the reaction kinetics are still sluggish, with neither the [Low LiH/MgB_2] nor [High LiH/MgB_2] samples completely hydrogenating after 24 hours of the HP hydrogenation. No partially hydrogenated B_xH_y species are formed during the hydrogenation, indicating direct conversion of the precursor LiH-MgB_2 state to borohydride. XRD and NMR evidence is reported for a mixed metal borohydride of the type $Mg_{(3-x)/2}Li_x(BH_4)_3$ produced by the hydrogenation along with varying amounts of crystalline MgH_2. The production of a mixed metal borohydride seems like a natural result of high-

temperature hydrogenation of the precursor LiH-MgB_2 state (Fig. 5) since Li has substituted for Mg and can interact with B. Also, the formation of MgH_2 and borohydride are natural consequences of the H-Mg interaction and the proximity of H to B in the proposed precursor structure. Eutectic melting influences the physical characteristics of the reaction products.

Hydrogen Desorption:

The materials produced by the HP hydrogenation were investigated for their ability to desorb hydrogen, thus measuring the extent of the hydrogenation achieved by the HP hydrogen treatment and testing the reversibility of the materials for hydrogen storage. Fig. 10 shows thermal desorption into static vacuum from [Low LiH/MgB_2 HP], [High LiH/MgB_2 HP Bottom] and [High LiH/MgB_2 HP Top] as they were heated to 385 °C with a ramp of 3 °C/min.

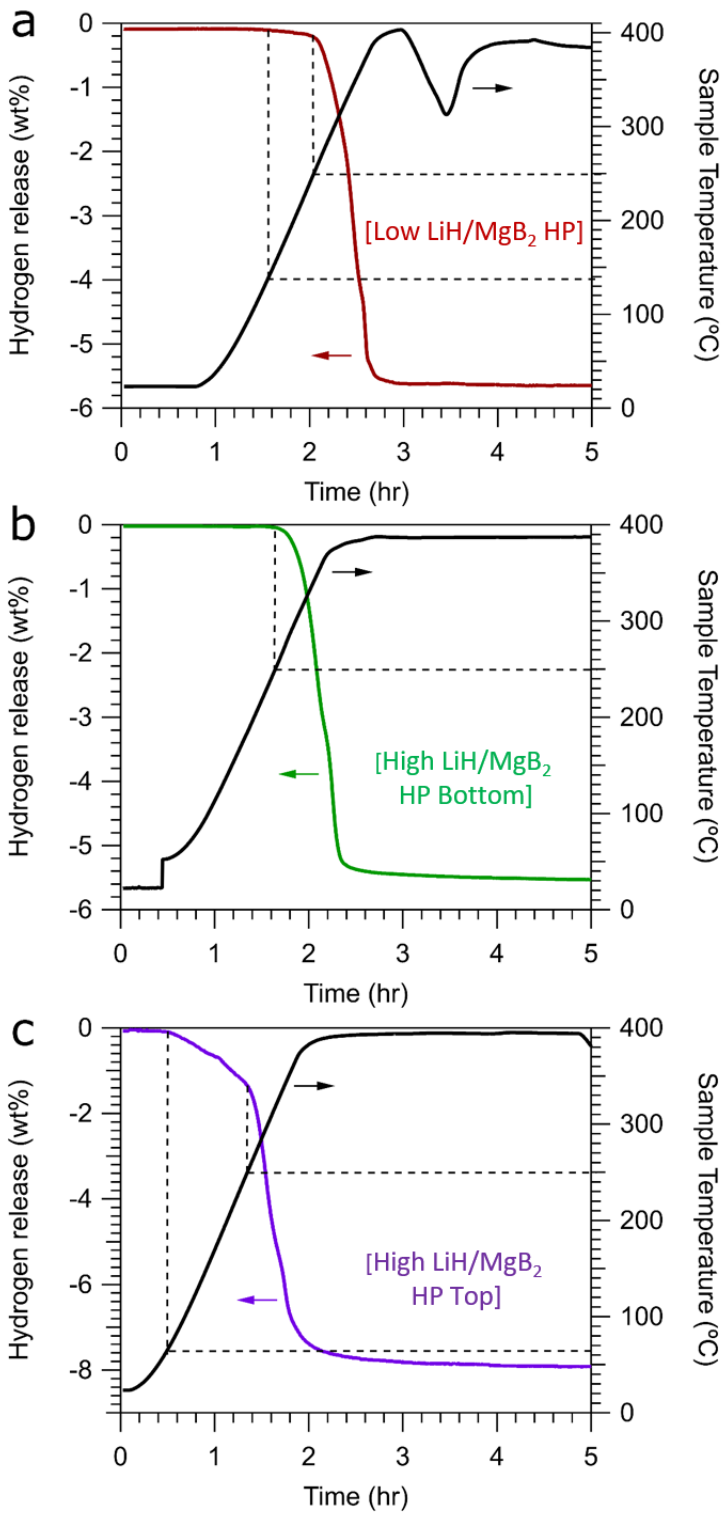

Fig. 10: Thermal desorption of hydrogen gas from the three HP hydrogenated samples; (a) [Low LiH/MgB_2 HP]; (b) [High LiH/MgB_2 HP Bottom] and (c) [High LiH/MgB_2 HP Top]. Desorption occurred into static vacuum with a temperature ramp of 3 °C/min. The dip in the temperature profile of panel (a) at 3.4 hours is an experimental heating artifact.

For [Low LiH/MgB_2 HP], 5.6 wt.% H is released. The onset of hydrogen desorption, defined here as the hydrogen release value increasing 0.02 wt.% above its initial baseline and indicated by the first dashed line in Fig. 10(a), is ~ 140 °C. The onset of rapid desorption occurs at ~250 °C. The [High LiH/MgB_2 HP Bottom] sample shows similar hydrogen release, with the onset for rapid hydrogen release occurring at ~ 250 °C with 5.5 wt.% H being desorbed. However, there is no low temperature onset at 140 °C as was seen for [Low LiH/MgB_2 HP] in Fig. 10(a). The [High LiH/MgB_2 HP Top] material releases 7.9 wt.% hydrogen with an onset of hydrogen desorption at a very low 65 °C followed by rapid hydrogen release at ~ 250 °C. In an overall sense, LiH promotes the kinetics of the hydrogen release. As apparent from Fig. 10, the average wt. % released per hour over the course of ~ 2 – 3 hours increases with LiH content, since the hydrogen desorption rate varies as: [Low LiH/MgB_2 HP] < [High LiH/MgB_2 HP Bottom] < [High LiH/MgB_2 HP Top].

XRD was used to probe for crystalline products created by the desorption, as shown in Fig. 11. We label the desorbed samples as follows: For desorption from [Low LiH/MgB_2 HP], [High LiH/MgB_2 HP Top] and [High LiH/MgB_2 HP Bottom], we have, respectively, the desorbed samples [Low LiH/MgB_2 HPD], [High LiH/MgB_2 HPD Top] and [High LiH/MgB_2 HPD Bottom].

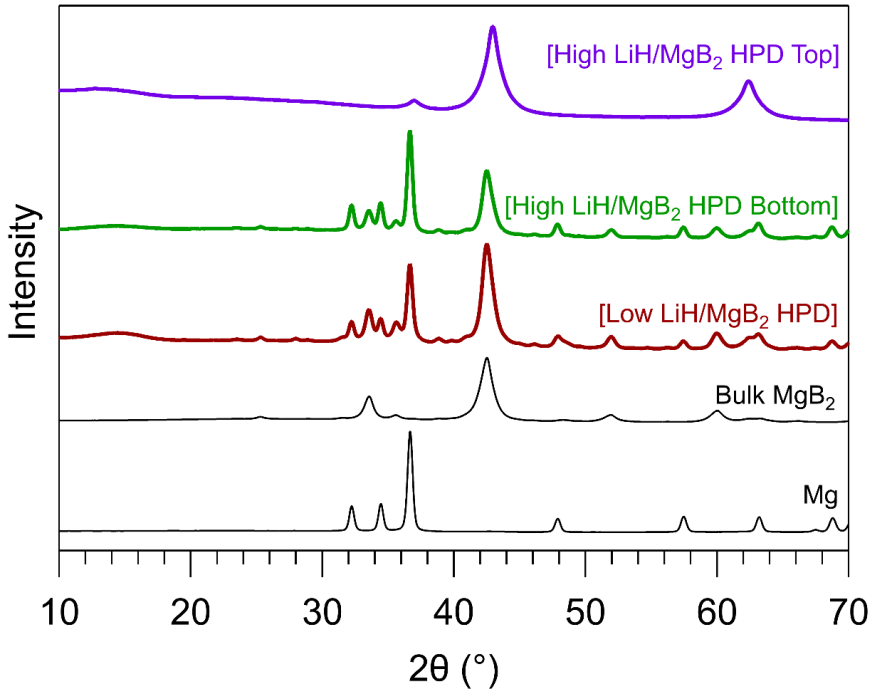

Fig. 11: XRD of HP hydrogenated samples after undergoing thermal desorption into static vacuum up to 385 °C: [Low LiH/MgB_2 HPD], [High LiH/MgB_2 HPD Bottom] and [High LiH/MgB_2 HPD Top] are compared to Mg metal and Bulk MgB_2 standards.

For [Low LiH/MgB_2 HPD], borohydride crystalline peaks have disappeared upon desorption, producing two major crystalline phases: Mg metal and MgB_2. There is no sign of β-MgH_2 (peaks that would appear at 28° and 35.8°), as the temperature of the desorption is sufficient for MgH_2 dissociation [60]. Similar results are seen for [High LiH/MgB_2 HPD Bottom] where borohydride peaks all disappear upon desorption, leading to crystalline phases of Mg metal and MgB_2. An unknown phase is observed in [High LiH/MgB_2 HPD Top] which does not match Mg, MgB_2, or elemental boron [61]. This unknown phase also exists as a minority component of the other two "HPD" samples, suggesting that it plays a role in the desorption of all LiH-MgB_2 samples.

The desorbed samples were examined with FTIR to search for possible amorphous desorption products that would not be detected by XRD, as shown in Fig. 12.

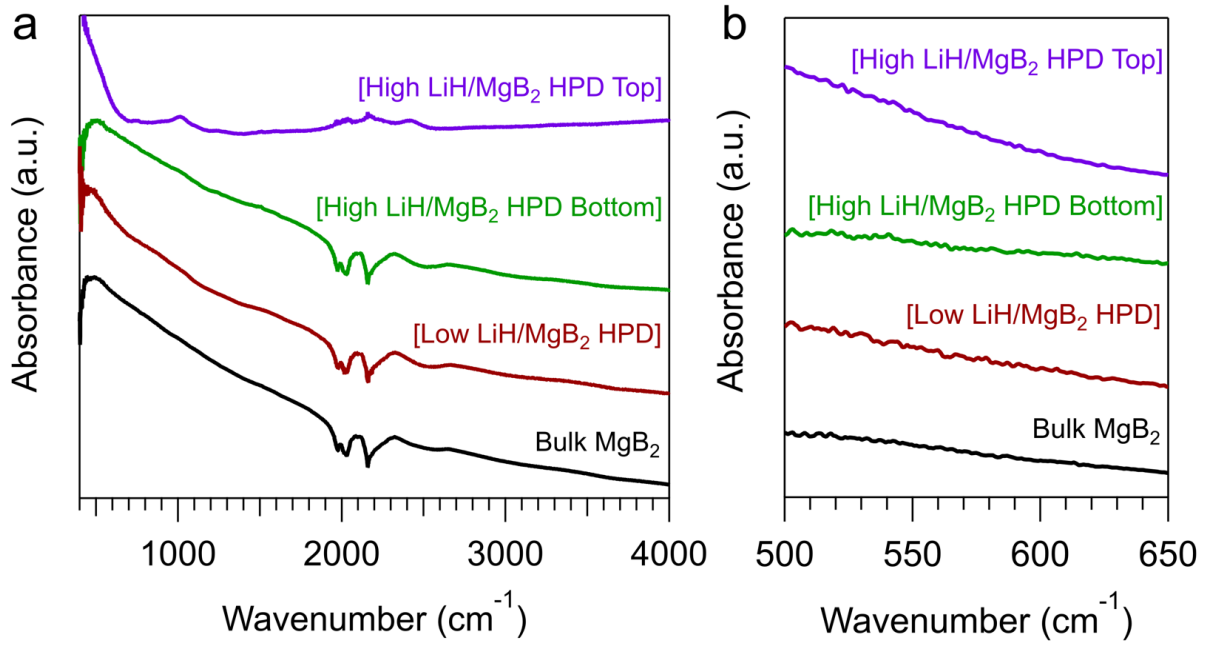

Fig. 12: FTIR spectra for [Low LiH/MgB_2 HPD], [High LiH/MgB_2 HPD Bottom] and [High LiH/MgB_2 HPD Top] (a) FTIR spectrum from 400 – 4000 cm^{-1}; (b) same data plotted with an expanded abscissa from 500 – 650 cm^{-1} where no evidence for the LiH vibrational feature at 550 cm^{-1} is seen.

For all of the samples, the borohydride features disappear upon desorption. There is no evidence for partially dehydrogenated boron species B_xH_y in the 2100 – 2400 cm^{-1} range which could have been produced by intermediate species that inhibit full hydrogen desorption. Thus, the combined XRD and FTIR results indicate there is no hydrogen remaining in the sample after heating to 385 ºC. The FTIR features between 650 cm^{-1} and 800 cm^{-1} (Fig. 7(b)) which are characteristic of lithium borate also disappear with desorption (Fig. 12(a)). This phenomenon will be discussed

more fully in the companion study (II) [34]. There is no sign of LiH in the FTIR (Fig. 12(b)) which indicates the system is not reversible since LiH/MgB_2 is not regenerated by the hydrogen desorption.

The desorption data are quite different from that reported in the literature for pure $Mg(BH_4)_2$ and $LiBH_4$ as well as for a eutectic mixture of these borohydrides. Soloveichick et al. [48] reports a series of steps in the hydrogen desorption from pure $Mg(BH_4)_2$ corresponding to the production of different B_xH_y intermediates. In addition, there is still hydrogen in the $Mg(BH_4)_2$ sample at 400 °C, and it takes heating the sample to 500 °C to release all the hydrogen. For $LiBH_4$, Guo et al. [62] report that hydrogen thermally desorbs in a step-wise fashion, with only 2 wt.% H desorbing up to 450 °C. The FTIR and XRD data show that there are no hydrogen-containing species left in the hydrogenated LiH/MgB_2 samples after heating to 385 °C. Multiple desorption steps were also seen in a 1:1 eutectic mixture of $Mg(BH_4)_2$ and $LiBH_4$, with a lowered hydrogen desorption onset of 170 °C [26]. In contrast, desorption from the hydrogenated samples [Low LiH/MgB_2 HP], [High LiH/MgB_2 HP Bottom] and [High LiH/MgB_2 HP Top] seems to be completed in one step, although the desorption from [High LiH/MgB_2 HP Top] does have a very low temperature onset of 65 °C which appears to be a precursor step to the main hydrogen desorption. One difference between the hydrogenated LiH/MgB_2 samples in the present study and those of eutectic mixture is that the eutectic mixture of $Mg(BH_4)_2$ and $LiBH_4$ showed no evidence for the mixed metal borohydride $Mg_{(3-x)/2}Li_x(BH_4)_3$ [26]. This mixed metal borohydride may be responsible for the rapid single-step release of hydrogen from the hydrogenated LiH/MgB_2 system studied here.

The desorption results for the [Low LiH/MgB_2 HP], [High LiH/MgB_2 HP Bottom] and [High LiH/MgB_2 HP Top] materials can be compared with prior studies [27, 28] of LiH combined with $Mg(BH_4)_2$. Yang et al. [27] found that for ball-milled LiH/$Mg(BH_4)_2$ with Li/Mg ratio of 0.3, thermal desorption of hydrogen occurred in multiple steps (producing B_xH_y intermediates) at 245 °C, 306 °C and 332 °C. In contrast, our [Low LiH/MgB_2 HP] material with Li/Mg ratio of 0.2 shows a single step release at 250 °C, with an onset at 140 °C (Fig. 10(a)). For higher LiH loadings, Yang et al. [27] find a single-step hydrogen release at 210 °C, with an onset of 150 °C, releasing a total of 12.5 wt. % when heated to 450 °C. In another study, Grube et al. [28] found that a physical mixture of LiH/$Mg(BH_4)_2$ made by mortar and pestle grinding with a Li/Mg ratio of 0.5 released hydrogen via multiple steps, with an onset of ~ 250 °C. These prior results for 0.5 LiH/$Mg(BH_4)_2$ differ from our [High LiH/MgB_2 HP Top] sample, which releases 7.9 wt. % hydrogen at 250 °C with an onset of 65 °C.

There are enough differences between the hydrogen desorption data from the LiH/MgB_2 HP hydrogenated samples and prior work [27, 28] to suggest that the [Low LiH/MgB_2 HP] and [High LiH/MgB_2 HP Top] samples are not the same material species as those releasing hydrogen in the prior studies. It's possible that the mixed metal borohydride $Mg_{(3-x)/2}Li_x(BH_4)_3$ found in our work is not produced in these prior studies because they used $Mg(BH_4)_2$ (as opposed to

MgB_2) as the starting point in the original mixing with LiH. No mention of a mixed-metal borohydride is made in the prior studies [27, 28].

The reader is referred to the companion study (II) [34] for a study of the surface and near-surface phenomena occurring in the LiH/MgH_2 hydrogen storage system as it undergoes the HP-hydrogenation/dehydrogenation cycle.

Future Work

Future work needs to focus on a better understanding of the precursor $LiH\text{-}MgB_2$ state, the reaction taking place between LiH and MgB_2 during the hydrogenation to form the mixed-metal borohydride, and the relative amounts of $Mg_{(3-x)/2}Li_x(BH_4)_3$, $Mg(BH_4)_2$ and $LiBH_4$ that may co-exist. NMR will be a very productive tool to identify and discriminate the identities and amounts of possible hydrogenation products. A deeper follow-on study involving systematic variation of the amount of added LiH, changing HP hydrogenation temperature and performing deconvolution analyses of the NMR lineshapes would clarify the nature of the broadened ^7Li, ^1H and ^{11}B NMR peaks produced by HP hydrogenation. Such a study was beyond the scope of the current investigation.

The composition and structure of the mixed metal borohydride needs to be elucidated. We note that the identifications of the mixed metal borohydride $Mg_{(3-x)/2}Li_x(BH_4)_3$ made here have been so assigned in part because the XRD and NMR results differ from the pure substances $Mg(BH_4)_2$ and $LiBH_4$. Such spectral assignments could be placed on a more solid footing if more experimental characterization data were gathered for pure mixed metal borohydrides. Strategies for improving the reversibility of the LiH/MgB_2 material will be pursued. Finally, ongoing theoretical work, the subject of a future publication, will investigate the energetics and structural consequences of adding LiH to MgB_2 for the purposes of storing hydrogen.

Conclusions

The influence of LiH and TiH_2 on the hydrogen storage reactions of MgB_2 were investigated. The results show that for ball-milled mixtures of LiH/MgB_2 the LiH forms a weakly-bound complex with MgB_2. While LiH addition leads to minor influence on the local B and Mg electronic structure, the B-B ring signature is not significantly altered and the hexagonal MgB_2 crystal structure persists. The weakly interacting $LiH\text{-}MgB_2$ complex state is not a mixed-metal boride of the type $Mg_{1-x}Li_xB_2$ and is additionally characterized by XPS in the companion study (II) and theoretically in current studies in progress.

Despite such weak interactions between LiH and MgB_2 in the initial state, a dramatic improvement is seen for the hydrogenation of MgB_2 at 280 °C and 700 bar. It is unclear at present if this is primarily a thermodynamic or kinetic effect. With LiH additive, MgB_2

hydrogenates to borohydride at least 100 ºC lower than pure MgB_2. Furthermore, evidence is found for a mixed metal borohydride $Mg_{(3-x)/2}Li_x(BH_4)_3$ produced by the hydrogenation. The species $Mg_{(3-x)/2}Li_x(BH_4)_3$ should play a role in any hydrogenation of a mixture of LiH and MgB_2, which is the dehydrogenated state of the $LiBH_4$ system destabilized with MgH_2. The thermodynamics of the mixed-metal borohydride are unknown, but would be important for a thermodynamic accounting of the MgH_2-destabilized $LiBH_4$ material which to date has been described (in the hydrogenated state) as a mixture of $LiBH_4$ and MgH_2.

No partially hydrogenated closo-borate species such as $[B_3H_8]^-$, $[B_{10}H_{10}]^{2-}$ or $[B_{12}H_{12}]^{2-}$ are formed, indicating hydrogenation of LiH/MgB_2 proceeds without the formation of undesirable intermediates, which itself is a substantial improvement in hydrogen storage. Instead of a step-wise series of desorptions characteristic of pure $Mg(BH_4)_2$ and $LiBH_4$ leading to different B_xH_y intermediates, desorption from $Mg_{(3-x)/2}Li_x(BH_4)_3$ releases up to 7.9 wt.% hydrogen in one step, with no hydrogen remaining in the sample by 380 ºC. By contrast, the pure substances $Mg(BH_4)_2$ and $LiBH_4$ still retain significant amounts of hydrogen when heated to this temperature. Unfortunately, after heating to 380 ºC, the $Mg_{(3-x)/2}Li_x(BH_4)_3$ material post desorption does not correspond to the starting material made by ball milling together LiH and MgB_2, with substantial amounts of Mg metal being produced along with MgB_2, and no regeneration of LiH. Thus, the material is not fully reversible.

In contrast to LiH, TiH_2 is inert when combined with MgB_2 via ball milling. TiH_2 had been predicted to produce strong destabilization in $LiBH_4$ and the reaction $TiH_2 + MgB_2 \rightarrow TiB_2 + MgH_2$ has a favorable ΔH_{rxn} of -118.38 kJ/mole, providing hope that TiH_2 could be a source of potent B-B ring disruption in MgB_2. This hope was not realized. Our results are similar to prior experiments involving $LiBH_4$ and $NaBH_4$ with TiH_2, for which TiH_2 was found to be unreactive.

Acknowledgements

The authors acknowledge financial support through the Hydrogen Storage Materials Advanced Research Consortium (HyMARC) of the U.S. Department of Energy (DOE), Office of Energy Efficiency and Renewable Energy, Fuel Cell Technologies Office under Contracts DE-AC52-07NA27344 and DE-AC04-94AL85000. Part of the work was performed under the auspices of the DOE by Lawrence Livermore National Laboratory under Contract DE-AC52-07NA27344. Sandia National Laboratories is a multi-mission laboratory managed by National Technology and Engineering Solutions of Sandia, LLC, a wholly owned subsidiary of Honeywell International Inc., for the DOE's National Nuclear Security Administration under contract DE-NA0003525. Portions of this research were performed on BLs 6.3.1.2 and 8.0.1.1 at the Advanced Light Source, Lawrence Berkeley National Laboratory, which is supported by the Director, Office of Science, Office of Basic Energy Sciences, of the U.S. DOE under Contract DE-AC02–05CH11231. The authors acknowledge Robert Horton for acquiring the Sieverts

desorption data, and Brendan Davis for assistance with the HP hydrogenation experiments. Thanks are extended to Sonjong Hwang of The California Institute of Technology for helpful communications regarding LiH NMR.

LLNL-JRNL-823824-DRAFT.

References:

(1) Bannenberg, L.J.; Heere, M.; Benzidi, H.; Montero, J.; Dematteis, E.M.; Suwarno, "Metal (boro-) Hydrides for High Energy Density Storage and Relevant Emerging Technologies," *Int. J. Hydrogen Energy **45** (2020) 33687-33730.*

(2) Milanese, C.; Jensen, T.R.; Hauback, B.; Pistidda, C.; Dornheim, M.; Yang, H., "Complex Hydrides for Energy Storage, *Int. J. Hydrogen Energy **44** (2019) 7860 – 7874.*

(3) Nagamatsu, J.; Nakagawa, N.; Muranaka, T.; Zenitani, Y.; Akimitsu, J. Superconductivity at 39 K in Magnesium Diboride. *Nature* **2001**, *410* (6824), 63–64.

(4) Pistidda, C.; Santhosh, A.; Jerabek, P.; Shang, Y.; Girella, A.; Milanese, C.; et al. "Hydrogenation Via a Low Energy Mechanochemical Approach: The MgB_2 Case," *J. Phys. Energy **3** (2021) 044001 1-3.*

(5) Zavorotynska, O.; El-Kharbachi, A.; Deledda, S.; Hauback, B. C. Recent Progress in Magnesium Borohydride $Mg(BH_4)_2$: Fundamentals and Applications for Energy Storage. *Int. J. Hydrogen Energy* **2016**, *41* (32), 14387–14403.

(6) Sugai, C.; Kim, S.; Severa, G.; White, J. L.; Leick, N.; Martinez, M. B.; Gennett, T.; Stavila, V.; Jensen, C. Kinetic Enhancement of Direct Hydrogenation of MgB_2 to Mg(BH4)2 upon Mechanical Milling with THF, MgH_2, and/or Mg. *ChemPhysChem* **2019**, *20* (10), 1301–1304.

(7) Ray, K. G.; Klebanoff, L. E.; Lee, J. R. I.; Stavila, V.; Heo, T. W.; Shea, P.; Baker, A. A.; Kang, S.; Bagge-Hansen, M.; Liu, Y. S.; White, J. L.; Wood, B. C. Elucidating the Mechanism of MgB_2 Initial Hydrogenation via a Combined Experimental-Theoretical Study. *Phys. Chem. Chem. Phys.* **2017**, *19* (34), 22646–22658.

(8) Vajo, J. J.; Tan, H.; Ahn, C. C.; Addison, D.; Hwang, S.-J.; White, J. L.; Wang, T. C.; Stavila, V.; Graetz, J. Electrolyte-Assisted Hydrogen Storage Reactions. *J. Phys. Chem. C* **2018**, *122* (47), 26845–26850.

(9) Liu, Y. S.; Klebanoff, L. E.; Wijeratne, P.; Cowgill, D. F.; Stavila, V.; Heo, T. W.; Kang, S.; Baker, A. A.; Lee, J. R. I.; Mattox, T. M.; Ray, K. G.; Sugar, J. D.; Wood, B. C. Investigating Possible Kinetic Limitations to MgB_2 Hydrogenation. *Int. J. Hydrogen Energy* **2019**, *44* (59), 31239–31256.

(10) Paskevicius, M.; Jepsen, L. H.; Schouwink, P.; Černý, R.; Ravnsbæk, D. B.; Filinchuk, Y.; Dornheim, M.; Besenbacher, F.; Jensen, T. R. Metal Borohydrides and Derivatives-Synthesis, Structure and Properties. *Chem. Soc. Rev.* **2017**, *46* (5), 1565–1634.

(11) Pistidda, C.; Garroni, S.; Dolci, F.; Bardají, E. G.; Khandelwal, A.; Nolis, P.; Dornheim, M.; Gosalawit, R.; Jensen, T.; Cerenius, Y.; Suriñach, S.; Baró, M. D.; Lohstroh, W.; Fichtner, M. Synthesis of Amorphous $Mg(BH_4)_2$ from MgB_2 and H_2 at Room Temperature. *J. Alloys Compd.* **2010**, *508* (1), 212–215.

(12) Severa, G.; Rönnebro, E.; Jensen, C. M. Direct Hydrogenation of Magnesium Boride to Magnesium Borohydride: Demonstration of >11 Weight Percent Reversible Hydrogen Storage. *Chem. Commun.* **2010**, *46* (3), 421–423.

(13) Newhouse, R.J.; Stavila, V.; Hwang, S.J.; Klebanoff, L.E.; Zhang, J.Z. Reversibility and Improved Hydrogen Release of Magnesium Borohydride, J. Phys. Chem. C **114** (2010) 5224 – 5232.

(14) Barkhordarian, G.; Klassen, T.; Dornheim, M.; Bormann, R. Unexpected Kinetic Effect of MgB_2 in Reactive Hydride Composites Containing Complex Borohydrides. *J. Alloys Compd.* **2007**, *440* (1–2).

(15) Vajo, J. J.; Skeith, S. L.; Mertens, F. Reversible Storage of Hydrogen in Destabilized $LiBH_4$. *J. Phys. Chem. B* **2005**, *109* (9), 3719–3722.

(16) S. Kumar, U. Jain, A. Jain, H. Miyaoka, T. Ichikawa, Y. Kojima and G.K. Dey, "Development of Mg-Li-B Based Advanced Material for Onboard Hydrogen Storeage Solution," Int. J. Hydrogen Energy **42** (2017) 3963 – 3970.

(17) Saldan, I.; Campesi, R.; Zavorotynska, O.; Spoto, G.;Baricco, M.; Arendarska, A.; Taube, K. and Dornheim, M. Enhanced Hydogen Uptake/Release in $2LiH-MgB_2$ Composite with Titanium Additives. *Int. J. Hydrogen Energy* **2012,** *37*, 1604 – 1612.

(18) J.Z. Hu, J.H. Kwak, Z. Yang, X. Wan and L.L. Shaw "Detailed Investigation of Ion Exchange in Ball-milled $LiH+MgB_2$ System with Ultra-high Field Nuclear Magnetic Resonance Spectroscopy," J. Power Sources **195** (2010) 3645 – 3648.

(19) J.Z. Hu, J.H. Kwak, Z. Yang, X. Wan and L.L. Shaw, "Direct Observation of Ion Exchange in Mechanically Activated $LiH + MgB_2$ System using Ultrahigh Field Nuclear Magnetic Resonance Spectroscopy," App. Phys. Lett. **94** (2009) 141905 1- 3.

(20) J. Karpinski, N.D. Zhigadlo, S. Katrych, R. Puzniak, K. Rogacki and R. Gonnelli, "Single Crystals of MgB_2: Synthesis, Substitutions and Properties," Physica C **456** (2007) 3 – 13.

(21) X.S. Wu and J. Gao, "Heat of Formation in (Mg,X)B_2 (X = Li, Na, Ca, Al)," Physica C **418** (2005) 151 – 159.

(22) Y.G. Zhao, X.P. Zhang, P.T. Qiao, H.T. Zhang, S.L. Jia, B.S. Cao, M.H. Zhu, Z.H. Han, X.L. Wang and B.L. Gu, "Effect of Li Doping on Structure and Superconducting Transition Temperature of $Mg_{1-x}Li_xB_2$," Physica C **361** (2001) 91 – 94.

(23) Z.-Z. Fang, X.-D. Kang, P. Wang, H.-W. Li and S.-I. Orimo, "Unexpected Dehydrogenation Behavior of $LiBH_4/Mg(BH_4)_2$ Mixture Associated with the In-situ Formation of Dual-cation Borohydride," J. Alloys and Compounds **491** (2010) L1 – L4.

(24) L. Silvi, Z. Zhao-Karger, E. Röhm, M. Fichtner, W. Petry and W. Lohstroh, "A Quasielastic and Inelastic Neutron Scattering Study of Alkaline and Alkaline Earth Borohydrides $LiBH_4$ and $Mg(BH_4)_2$ and the Mixture $LiBH_4 + Mg(BH_4)_2$," Phys. Chem. Chem. Phys. **21** (2019) 718 – 728.

(25) Z. Zhao-Karger, R. Witter, E.G. Bardaji, D. Wang, D. Cossement and M. Fichtner, "Altered Reaction Pathways of Eutectic $LiBH_4$-$Mg(BH_4)_2$ by Nanoconfinement," J. Mater. Chem. A **1** (2013) 3379 – 3386.

(26) E.G. Bardaji, Z. Zhao-Karger, N. Boucharat, A. Nale, M.J. van Setten, W. Lohstroh, E. Röhm, M. Catti and M. Fichtner, "$LiBH_4$-$Mg(BH_4)_2$: A Physical Mixture of Metal Borohydrides as Hydrogen Storage Material," J. Phys. Chem. C **115** (2011) 6095 – 6101.

(27) J. Yang, H. Fu, P. Song, J. Zheng and X. Li, "Reversible Dehydrogenation of $Mg(BH_4)_2$-LiH Composite Under Moderate Conditions," Int. J. Hydrogen Energy **37** (2012) 6776 – 6783.

(28) E. Grube, S.R.H. Jensen, U.G. Nielsen and T.R. Jensen, "Reactivity of Magnesium Borohydride-Metal Hydride Composites, γ-$Mg(BH_4)_2$-MH_x, M = Li, Na, Mg, Ca," J. Alloys and Compounds **770** (2019) 1155 – 1163.

(29) J. Puszkiel, A. Gasnier, G. Amica and F. Gennari, "Tuning $LiBH_4$ for Hydrogen Storage: Destabilization, Additive, and Nanoconfinement Approaches," Molecules **25** (2020) 163.

(30) Zhang, Y.; Morin, F.; Huot, J. The Effects of Ti-based Additives on the Kinetics and Reactions in LiH/MgB_2 Hydrogen Storage System, Int. J. Hydrogen Energy **36** (2011) 5425-5430.

(31) D.J. Siegel, C. Wolverton and V. Ozolins, "Thermodynamic Guidelines for the Prediction of Hydrogen Storage Reactions and Their Application to Destabilized Hydride Mixtures," Phys. Rev. B **76**, 134102 (2007).

(32) J. Yang, A. Sudik and C. Wolverton, "Destabilizing $LiBH_4$ with a Metal (M= Mg, Al, Ti, V, Cr or Sc) or Metal Hydride (MH_2 = MgH_2, TiH_2 or CaH_2)," J. Phys. Chem. C **111** (2007) 19134 – 19140.

(33) S. Garroni, C. Milanese, A. Girella, A. Marini, G. Mulas, E. Menendez, C. Pistidda, M. Dornheim, S. Surinach and M.D. Baro, "Sorption Properties of $NaBH_4/MH_2$ (M = Mg, Ti) Powder Systems," Int. J. Hydogen Energy **35** (2010) 5434 – 5441.

(34) J.L. Snider, T.M. Mattox, Y.-S. Liu, L.F. Wan, P. Wijeratne, M.D. Allendorf, V. Stavila,

B.C. Wood and L.E. Klebanoff, *"The Influence of LiH and TiH_2 on Hydrogen Storage in MgB_2 II. XPS Study of Surface and Near-surface Phenomena,"* International Journal of Hydrogen Energy **XX** (2021) yyy – zzz.

(35). Y.-S. Liu, K.G. Ray, M. Jørgensen, T.M. Mattox, D.F. Cowgill, H.V. Eshelman, A.M. Sawvel, J.L. Snider, W. York, P. Wijeratne, A.M. Pham, H. Gunda; S. Li, T.W. Heo, S. Kang, T.R. Jensen, S. Stavila, B.C. Wood and L.E. Klebanoff, "Nanoscale Mg-B Via Surfactant Ball Milling of MgB_2: Morphology, Composition and Improved Hydrogen Storage Properties" J. Phys. Chem. C **124** (2020) 21761-21771.

(36) Kohn, W.; Sham, L. J. *"Self-consistent Equations Including Exchange and Correlation Effects,"* Phys. Rev. **140** (1965) A1133 – A1138.

(37) Kresse, G.; Furthmuller, J. *"Efficiency of ab-initio Total Energy Calculations for Metals and Semiconductors Using a Plane-wave Basis Set,"* Comput. Mater. Sci. 6 (1996), 15 - 50.

(38) Kresse, G.; Hafner, J., *"Ab-initio Molecular Dynamics for Liquid Metals,"* Phys. Rev. B. **47** (1993) 558 - 561.

(39). P.E. Blöchl, *"Projector Augmented-wave Method,"* Phys. Rev. B **50** (1994) 17953 - 17979.

(40). Kresse, G.; Joubert, D., *"From Ultrasoft Pseudopotentials to the Projector Augmented-wave Method,"* Phys. Rev. B **59** (1999), 1758 - 1775.

(41). Perdew, J. P.; Burke, K.; Ernzerhof, M., *"Generalized Gradient Approximation Made Simple,"* Phys. Rev. Lett. **77** (1996) 3865 – 3868.

(42.) Nose, S., *"A Unified Formulation of the Constant Temperature Molecular Dynamics Methods,"* J. Chem. Phys. **81** (1984) 511 – 519.

(43). Hoover, W. G., *"Canonical Dynamics: Equilibrium Phase-space Distributions,"* Phys. Rev. A. **31** (1985) 1695 – 1697.

(44) Standard enthalpies of formation for TiH_2, MgB_2, TiB_2 and MgH_2 required as input to calculate ΔH_{rxn} were taken from the NIST Chemistry Webbook: https://webbook.nist.gov/chemistry/

(45). A. Sifuentes, A.C. Stowe and N. Smyrl, "Determination of the Role of Li_2O in the Corrosion of Lithium Hydride," J. Alloys and Cmpds. **580** (2013) S271-S273.

(46). X. Wang and L. Andrews, "Infrared Spectra and Theoretical Calculations of Lithium Hydride Clusters in Solid Hydrogen, Neon and Argon," J. Phys. Chem. A **111** (2007) 6008-6019.

(47). R.C. Bowman, Jr., S.-J. Hwang, C.C. Ahn and J.J. Vajo, *"NMR and X-ray Diffraction Studies of Phases in the Destabilized LiH-Si System,"* Mater. Res. Soc. Symp. Proc. **837** (2005) N3.6.1-N3.6.6.

(48) G.L. Soloveichik, Y. Gao, J. Rijssenbeek, M. Andrus, S. Kniajanski, R.C. Bowman Jr., S-J. Hwang and J.-C. Zhao, "Magnesium Borohydride as a Hydrogen Storage Material: Properties and Dehydrogenation Pathway of Unsolvated $Mg(BH_4)_2$," Int. J. Hydrogen Energy **34** (2009) 916-928.

(49). O. Friedrichs, A. Remhof, S.-J. Hwang and A. Zuttel, "The Role of $Li_2B_{12}H_{12}$ for the Formation and Decomposition of $LiBH_4$," Chem. Mater. **22** (2010) 3265 – 3268.

(50). S.-J. Hwang, R.C. Bowman, Jr., J.W. Reiter, J. Rijssenbeek, G.L Soloveichik, J.-C. Zhao, H. Kabbour and C.C. Ahn, *"NMR Confirmation for Formation of $[B_{12}H_{12}]^{2-}$ Complexes During Hydrogen Desorption from Metal Borohydrides,"* J. Phys. Chem. C **112** (2008) 3164 – 3169.

(51) J.-C. Zhao, D.A. Knight, G.M. Brown, C. Kim S.-J. Hwang, J.W. Reiter, R.C. Bowman, Jr., J.A. Zan and J.G. Kulleck, *"Study of Aluminoborane Compound AlB_4H_{11} for Hydrogen Storage,"* J. Phys. Chem. C **113** (2009) 2 – 11.

(52). Angeli, F.; Villain, O.; Schuller, S.; Charpentier, T.; De Ligny, D.; Bressel, L.; Wondraczek, L. Effect of Temperature and Thermal History on Borosilicate Glass Structure. *Phys. Rev. B - Condens. Matter Mater. Phys.* **2012**, *85* (5).

(53). Kroeker, S.; Stebbins, J. F. Three-Coordinated Boron-11 Chemical Shifts in Borates. *Inorg. Chem.* **2001**, *40* (24), 6239–6246.

(54). L. Lei, D. He, K. He, J. Qin, and S. Wang, *"Pressure-induced Coordination Changes in $LiBO_2$,"* J. Solid State Chemistry **182** (2009) 3041-3048.

(55). L. Duchene, R.-S. Kuhnel, D. Rentsch, A. Remhof, H. Hagemann and C. Battaglia, *"A Highly Stable Sodium Solid-state Electrolyte Based on a Dodeca/Deca-borate Equimolar Mixture,"* Chem. Commun. **53** (2017) 4195 – 4198.

(56). See the Main Article and Supporting Information for: H.-S. Lee, S.-J. Hwang, H.K. Kim, Y.-S. Lee, J. Park, J.-S. Yu and Y.W. Cho *"In Situ NMR Study of the Interaction Between $LiBH_4$-$Ca(BH_4)_2$ and Mesoporous Scaffolds,"* J. Phys. Chem. Lett. **3** (2012) 2922 – 2927.

(57). Y. Yan, H. Wang, M. Zhu, W. Cai, D. Rentsch and A. Remhof, *"Direct Rehydrogenation of $LiBH_4$ from H-Deficient $Li_2B_{12}H_{12-x}$,"* Crystals **8** (2018) 131-137.

(58). D. Ravnsbaek, Y. Filinchuk, Y. Cerenius, H.J. Jakobsen, F. Besenbacher, J. Skibsted and T.R. Jensen, *"A Series of Mixed-Metal Borohyrides,"* Angew. Chem. Int. Ed. **48** (2009) 6659 – 6663.

(59). D.B. Ravnsbaek, C. Frommen, D. Reed, Y. Filinchuk, M. Sorby, B.C. Hauback, H.J. Jakobsen, D. Book, F. Besenbacher, J. Skibsted and T.R. Jensen, *"Structural Studies of Lithium Zinc Borohydride by Neutron Powder Diffraction, Raman and NMR Spectroscopy,"* J. Alloys and Compounds **509S** (2011) S698 – S704.

(60). C. Zhou, C. Hu, Y. Li and Q. Zhang, *"Crystallite Growth Characteristics of Mg During Hydrogen Desorption of MgH_2,"* Progress in Natural Science: Materials International 30 (2020) 246 – 250.

(61). C.L. Turner, R.E. Taylor and R.B. Kaner *"^{10}B and ^{11}B NMR Study of Elemental Boron,"* J.

Phys. Chem. C **119** (2015) 13807 – 13813.

(62). L. Guo, L. Jiao, L. Li, Q. Wang, G. Liu, H. Du, Q. Wu, J. Du, J. Yang, C. Yan, Y. Wang and H. Yuan *"Enhanced Desorption Properties of $LiBH_4$ Incorporated Into Mesoporous TiO_2,"* Int. J. Hydrogen Energy **38** (2013) 162 – 168.